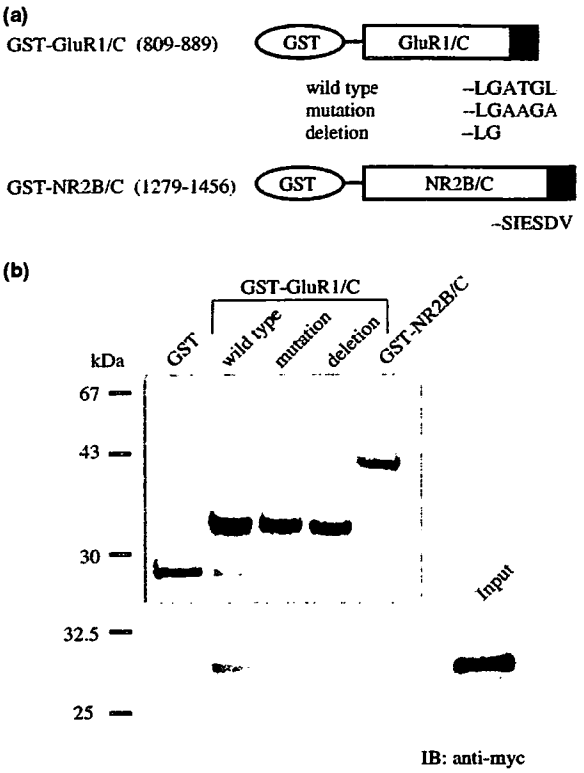

Fig. 3 Role of the post-synaptic density-95/Dlg/ZO-1 (PDZ) binding motif of GluR1 in the interaction with mouse Shank3 (mShank3)/SH3-PDZ. (a) The schematic description of glutathione S-transferase (GST)-fused GluR1/C and C-terminal segment of NMDA receptor 2B (NR2B/C) proteins. (b) Pull-down assay. The upper panel shows the purified GST and GST-fused proteins separated by sodium dodecyl sulfate–polyacrylamide gel electrophoresis (SDS–PAGE) and the lower panel shows the immunoblots. GST alone or each of the GST-fusion proteins bound to glutathione sepharose beads was incubated with 200 μg of extract from Chinese hamster ovary (CHO) cells transfected with myc-tagged mShank3/SH3-PDZ. After washing, the proteins on the beads were eluted with SDS–PAGE sample buffer and immunoblotted with anti-myc antibody. The input lane was loaded with 10 μg of the CHO cells extract. Molecular weight standards are shown on the left. SH3, Src homology 3; IB, immunoblot.

protein and coprecipitated GluR1 subunit, while normal IgG immunoprecipitated neither mShank3 nor GluR1 subunit. This finding suggests that mShank3 interacts with GluR1 AMPA receptor in mouse cortex.

We next used this antibody to examine cortical primary neurons for expression of mShank3 and the pattern of mShank3 immunoreactivity was found to be strikingly punctate. To clarify the distribution of mShank3, EGFP was transfected into neurons and its signal was superimposed on the mShank3 staining. As shown in Fig. 5(d), judging from their morphology mShank3 was mainly expressed in the spines. Moreover, the punctate signals of mShank3 closely coincided with those of PSD-95 (Fig. 5e), indicating that mShank3 was colocalized with PSD-95 in the spines.

Mouse Shank3 interacts with membrane-surface GluR1 subunit in the spines

As the GST pull-down and immunoprecipitation experiments demonstrated the biochemical interaction of mShank3 with GluR1 subunit, we investigated the interaction of these proteins in neurons. We constructed a plasmid, EGFP-GluR1, in which EGFP had been fused with the extracellular region of GluR1, and transfected it into cortical neurons cultured for 12 days. When we examined them 2 days later, the EGFP fluorescence perfectly matched the GluR1 staining (data not shown). Under permeant conditions, in which proteins located on both the intracellular and membrane surface are detected, immunostaining with anti-EGFP antibody revealed expression of EGFP-GluR1 in the cell body, neuritis and spines (Fig. 5f, i). By contrast, the EGFP-GluR1 staining was punctate when the anti-EGFP antibody was applied to a living culture under non-permeant conditions to detect EGFP-GluR1 delivered onto the membrane surface (Fig. 5f, ii), indicating that the membrane-surface EGFP-GluR1 forms clusters. Subsequent staining of the same neurons for PSD-95 under permeant conditions showed that the punctate EGFP-GluR1 staining coincided with the PSD-95 staining (Fig. 5f, iii), implying that the membrane-surface EGFP-GluR1 was distributed in the spines. This finding is consistent with previous reports that almost all membrane-surface GluR1 clusters are synaptic (Shi *et al.* 1999). At 2 days after cotransfection with myc-mShank3 and EGFP-GluR1, EGFP-GluR1 staining was performed with anti-EGFP antibody under non-permeant conditions and followed by myc-mShank3 staining with anti-myc antibody under permeant conditions. Many punctate myc-mShank3 staining signals were colocalized with those of EGFP-GluR1 staining (EGFP-GluR1/myc-mShank3 colocalization rate 80.0 ± 3.8%; $n = 5$) (Fig. 5g). At 1 week after cotransfection, the mShank3 staining was as strikingly punctate as native mShank3 staining and merged well with the EGFP-GluR1 staining in the spines (Fig. 5h). These results suggest that mShank3 interacts with membrane-surface GluR1 subunit.

All members of the mouse Shank family are expressed in the cortex and may interact with GluR1 subunit

Previous studies have shown that all three members of the Shank family are expressed in rat cortex. We investigated the expression and distribution of Shank mRNAs in the mouse cortex by *in situ* hybridization during post-natal development on post-natal days 1 and 15 and at 8 weeks of age. Antisense cRNA probes transcribed from each mShank gene specifically recognized particular mShank transcripts whereas sense cRNA probes did not (data not shown). As shown in Fig. 6(a), the hybridization signals for mShank1 and mShank2 mRNAs were detected at all post-natal stages

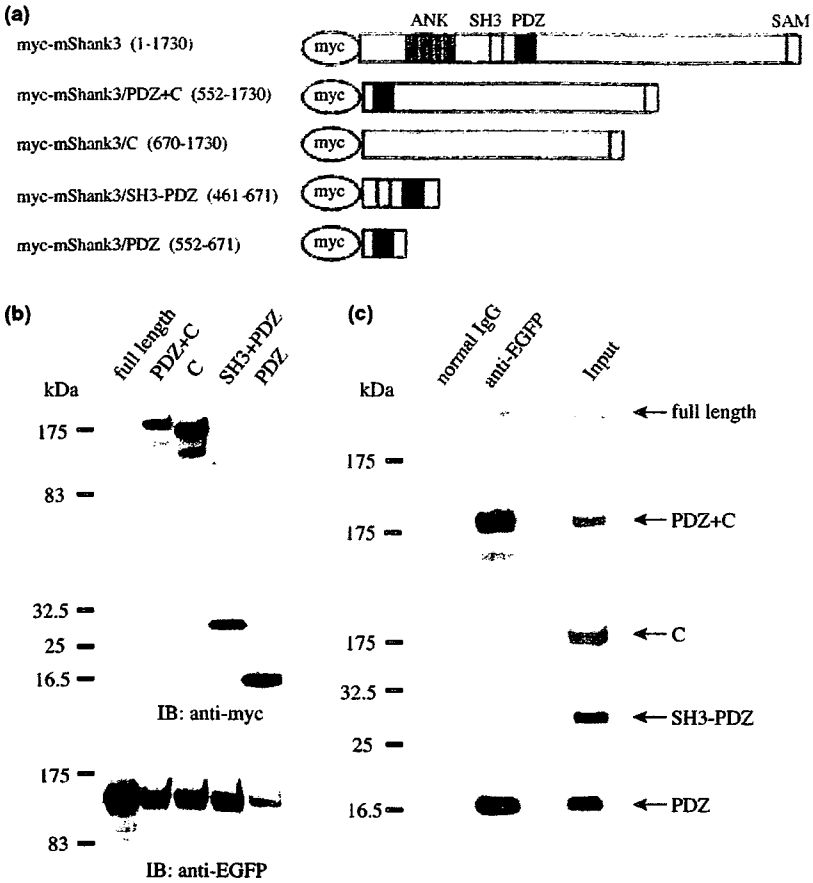

Fig. 4 GluR1 binds to the post-synaptic density-95/Dlg/ZO-1 (PDZ) domain of mouse Shank3 (mShank3). (a) Schematic structure of myc-tagged mShank3 mutants. (b) Immunoblot analysis. COS7 cells were transfected with each of the myc-tagged mShank3 mutants together with enhanced green fluorescent protein-fused GluR1 subunit (EGFP-GluR1). Lysates of transfected COS7 cells (5 μg of proteins) were separated by sodium dodecyl sulfate–polyacrylamide gel electrophoresis (SDS–PAGE) and immunoblotted with anti-myc antibody (upper panel) and with anti-enhanced green fluorescent protein (EGFP) antibody (lower panel). (c) Immunoprecipitation assay. Normal rabbit IgG or anti-EGFP antibody bound to Protein A- and G-Sepharose beads was incubated with 300 μg of extract from COS7 cells cotransfected with EGFP-GluR1 and myc-tagged mShank3 mutant. After washing, the proteins on the beads were eluted with SDS–PAGE sample buffer and immunoblotted with anti-myc antibody. Molecular weight standards are shown on the left. ANK, Ankyrin repeats 1–7; SH3, Src homology 3 domain; SAM, sterile alpha motif; IB, immunoblot.

measured; however, expression of mShank3 mRNA was clearly seen at post-natal days 1 and 15 and the signals at 8 weeks of age were very faint. These results were confirmed by RT-PCT (Fig. 6b) and immunoblot analysis (Fig. 6c). On the other hand, the distribution of the mRNAs of all members of the Shank family in the cortex was not significantly different. Thus, it appears that mShank1, mShank2 and mShank3 are expressed in the same neurons in cortex. Finally, we investigated whether mShank1 and mShank2 interact with GluR1 subunit, because the SH3-PDZ domain is well conserved among all members of the Shank family. As shown in Fig. 6(d), mShank1/SH3-PDZ and mShank2/SH3-PDZ also bound GluR1/C, the same as mShank3/SH3-PDZ.

Discussion

In this study we used a yeast two-hybrid screening system and identified a synaptic molecule that interacts with GluR1 subunit of AMPA receptors. The molecule, named Shank3/ProSAP2, is a multidomain protein localized in PSDs which links cell-surface receptors, including various types of GluRs, to the actin-based cytoskeleton (Lim *et al.* 1999; Naisbitt *et al.* 1999; Sheng and Kim 2000; Böckers *et al.* 2001, 2002). The most striking finding in our study was that GluR1 subunit is capable of directly binding to the PDZ domain of the Shank3 via its C-terminal PDZ-binding motif (four aa sequence, -ATGL), while GluR2 subunit indirectly binds to the SH3 domain of the Shank protein mediated by glutamate receptor-interacting protein (GRIP) (Sheng and Kim 2000). The PDZ domain is a stretch of 80–100 aa residues which plays an important role in protein–protein interaction (Songyang *et al.* 1997). Thus far it has been reported that synaptic proteins containing a type I PDZ-binding motif (the C-terminal four-amino-acid sequence -X-T/S-X-V/L/I, where X represents any aa), such as GKAP/SAP90/PSD-95-associated protein (SAPAP) (-QTRL), the somatostatin receptor 2 (-QTSI) and the calcium-independent α-latrotoxin receptor (-VTSL), bind to the PDZ domain of Shank (Böckers *et al.* 2002) and thus, the PDZ domain of Shank is thought to be a type I PDZ. As expected, no binding of the GluR2 subunit of AMPA receptors was observed in our study, as GluR2 subunit possesses a type II, not type I, PDZ-binding motif. Interestingly, however, little or no binding of the NR2B subunit was observed, even though NR2B subunit has a type I PDZ-binding motif

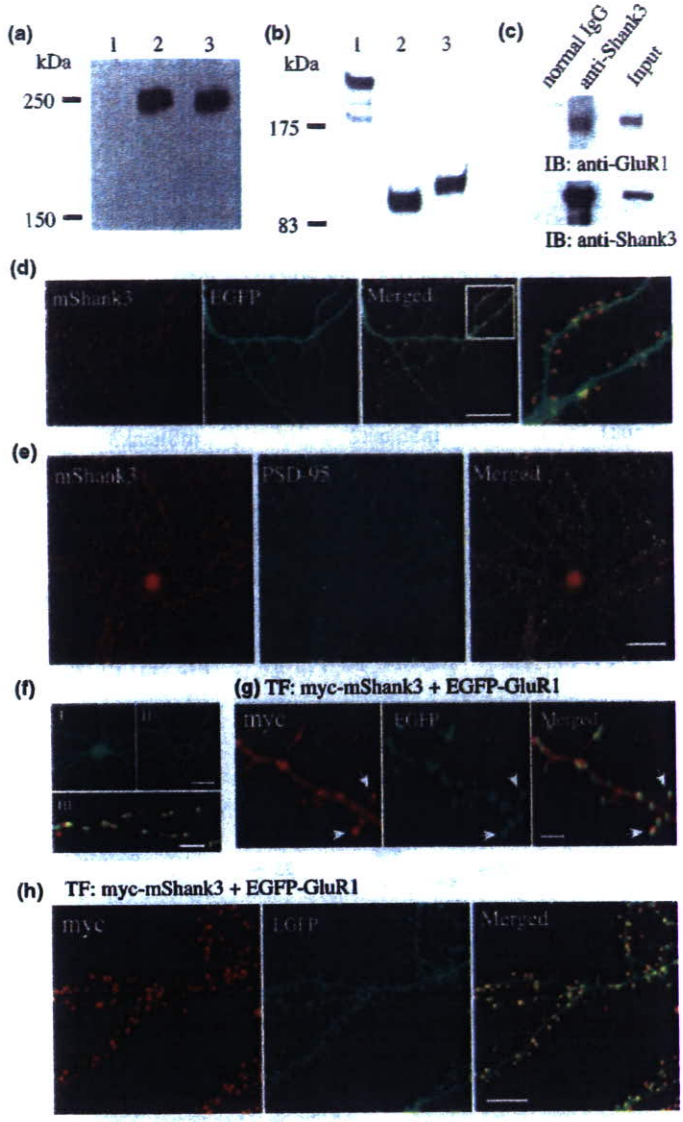

Fig. 5 Expression and distribution of mouse Shank3 (mShank3) in cortical neurons. (a) Immunoblot analysis. Lysates of COS7 cells (5 μg of proteins) transfected with myc (lane 1) or myc-mShank3 (lanes 2 and 3) were separated by sodium dodecyl sulfate–polyacrylamide gel electrophoresis (SDS–PAGE) and immunoblotted with anti-mShank3 antibody (lanes 1 and 2) and with anti-myc antibody (lane 3). (b) Immunoblot analysis. Synaptosomal proteins (30 μg) were separated by SDS–PAGE and immunoblotted with anti-mShank3 antibody (lane 1), anti-post-synaptic density-95 (PSD-95) antibody (lane 2) or anti-GluR1 antibody (lane 3). Molecular weight standards are shown on the left. (c) Immunoprecipitation assay. Normal rabbit IgG or anti-Shank3 antibody bound to Protein A- and G-Sepharose beads was incubated with 1 mg of membrane fraction from mouse cortex. After washing, the proteins on the beads were eluted with SDS–PAGE sample buffer and immunoblotted with anti-GluR1 antibody. The input lane was loaded with 50 μg of membrane fraction. (d) Cortical neurons cultured for 12 days were transfected with enhanced green fluorescent protein (EGFP). At 2 days later, the neurons were fixed and stained with anti-mShank3 antibody. An enlargement of the square field indicated is shown in the right panel. (e) Cortical neurons were cultured for 18 days and double-stained with anti-mShank3 antibody (red) and anti-PSD-95 antibody (green). (f) Cortical neurons cultured for 12 days were transfected with EGFP-fused GluR1 subunit (EGFP-GluR1). After 2 days, the neurons were stained with anti-EGFP antibody under permeant (i) or non-permeant (ii) conditions. The immunoreactive signals for anti-EGFP antibody (green) under non-permeant conditions were matched with those for anti-PSD-95 antibody (red) (iii). (g) Cortical neurons cultured for 12 days were transfected with myc-mShank3 and EGFP-GluR1. At 2 days later, the neurons were stained with anti-EGFP antibody (green) under non-permeant conditions and with anti-myc antibody (red) after fixation. The arrows point to examples of overlapping signals. (h) Cortical neurons cultured for 12 days were transfected with myc-mShank3 and EGFP-GluR1. At 7 days later, the neurons were stained with anti-EGFP antibody (green) and anti-myc antibody (red). Scale bars: 30 μm (d) and 15 μm (e, panels i and ii in f), 10 μm (h) and 5 μm (panel iii in f and g). IB, immunoblot; TF, transfection.

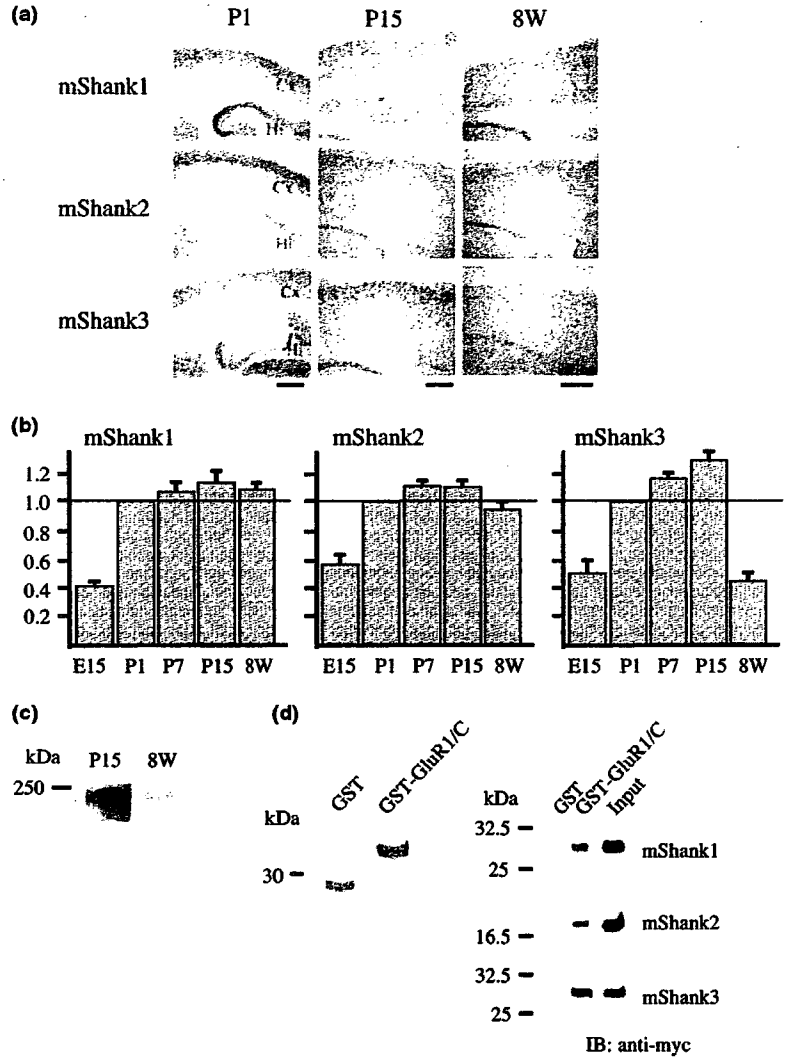

Fig. 6 Expression of mouse Shank (mShank) mRNAs in developing mouse cortex and interaction of mShank proteins with GluR1 subunit. (a) *In situ* hybridization analysis. Distribution of mShank mRNAs in the post-natal mouse cortex. Cx, cortex; Hi, hippocampus. Scale bar, 500 μm. (b) RT-PCR analysis. Amounts of total RNA used for the PCR were normalized to glyceraldehyde-3-phosphate dehydrogenase. The relative strength of the band signals was measured with NIH Imaging software and the ratio was calculated by dividing the value at each stage by the value at post-natal day (P)1. (c) Immunoblot analysis. Lysates of cortex (30 μg) prepared from P15 or 8-week-old mice were separated by sodium dodecyl sulfate–polyacrylamide gel electrophoresis (SDS–PAGE) and immunoblotted with anti-mShank3 antibody. (d) Pull-down assay. The left panel shows the purified glutathione S-transferase (GST) and GST-fused GluR1/C separated by SDS–PAGE and the right panels show the immunoblots. GST alone or GST-fused GluR1/C bound to glutathione sepharose beads was incubated with 300 μg of extract from Chinese hamster ovary (CHO) cells transfected with myc-tagged mShank/SH3-PDZ. After washing, the proteins on the beads were eluted with SDS–PAGE sample buffer and immunoblotted with anti-myc antibody. The input lane was loaded with 10 μg of the CHO cell extract. Molecular weight standards are shown on the left. PDZ, post-synaptic density-95/Dlg/ZO-1; SH3, Src homology 3 domain; 8W, 8 weeks of age; IB, immunoblot.

(-ESDV) by which NR2B subunit binds to the type I PDZ domain of PSD-95. The above findings suggest that the binding partners of Shank via the PDZ domain are highly selective molecules. A recent analysis of the crystal structure of the PDZ domain of the Shank–peptide ligand (EAQTRL) complex has revealed that the carboxylate binding loop formed by the second β-strand within the PDZ domain is critical for binding to the peptide ligand (Im *et al.* 2003). The aa sequence of the second β-strand is identical in all three members of the Shank family. The recent structural studies support our result showing that GluR1/C not only bound to Shank3 but also to Shank1 and Shank2.

The biochemical interaction of mShank3 with GluR1 subunit was complemented by coimmunoprecipitation assay with membrane fraction prepared from mouse cortex using anti-Shank3 antibody and by transfection experiments showing colocalization of Shank3 with GluR1 subunit in the spines of mouse cultured cortical neurons. When myc-mShank3 was expressed with EGFP-GluR1 in maturing cortical neurons, many myc-mShank3 clusters colocalized with cell-surface EGFP-GluR1. Shi *et al.* (1999) reported that cell-surface recombinant EGFP-GluR1, the same construct as our plasmid, expressed in hippocampal neurons displayed a punctate distribution that colocalized with both surface labeling of endogenous GluR2 subunit and with a pre-synaptic marker, synapsin. Therefore, our results suggest that myc-mShank3 colocalizes with functional AMPA receptors containing GluR1 subunit at synaptic sites.

Recent cumulative evidence has shown that the clustering of AMPA receptors at the post-synaptic membrane is critical for synaptic maturation and plasticity. As trafficking of GluR1 subunit to synapses was diminished by mutating the PDZ interacting region of GluR1 subunit, the trafficking may be mediated by a family of PDZ-domain-containing proteins (Hayashi *et al.* 2000; Shi *et al.* 2001). However, the binding partner of GluR1 subunit remains to be determined. One candidate is SAP-97, a type I PDZ protein homologous to PSD-95, and the biochemical interaction of SAP-97 with GluR1 subunit has actually been demonstrated (Leonard *et al.* 1998). During development, however, expression of SAP-97 is distributed more in the somatic region than in the dendrites, although it is found along dendrites, presumably at synaptic sites, in mature neurons (Valtschanoff *et al.* 2000). Thus, SAP-97 is thought to be associated with intracellular AMPA receptors, including GluR1 subunit, and to be involved in the early secretory pathway, endoplasmic reticulum/cis-Golgi pathway, of AMPA receptors trafficking during development (Sans *et al.* 2001). Shank3, on the other hand, is expressed in post-synaptic sites where the functional AMPA receptors are localized. Roussignol *et al.* (2005) recently showed that transfection of Shank3 into cerebellar granule cells increased the AMPA component of mEPSCs. Thus, Shank3 is an intriguing molecule that interacts with AMPA receptors and regulates their function at post-synaptic sites. The mechanism of activity-depending AMPA receptor trafficking to synapses involving Shank3 needs to be more thoroughly elucidated.

In situ hybridization and RT-PCR analyses have shown that Shank3 mRNA expression in mouse cortex increases after birth and gradually decreases during later development, consistent with previous studies on rat brain (Böckers *et al.* 2001, 2004). Thus, Shank3 may play an important role in neural functions, such as synaptogenesis and synapse maturation, at an early stage of post-natal development rather in adulthood. However, Shank1 and Shank2 mRNAs are also expressed in cortical neurons after birth and their expression levels are sustained into adulthood. Furthermore, the expression patterns of all three Shank mRNAs in the cortex do not significantly differ. The members of the Shank family share essentially the same domain structures, such as the SH3 and PDZ domains, and lower homologous regions, such as the proline-rich region. Thus, it has been thought that the individual members of the Shank family may have unique functions in addition to their common function as scaffold proteins but little is known about their other functions. Further study, especially in Shank knock-out and transgenic mouse, should provide useful insights into the functions of the individual members of the Shank family in regard to synaptogenesis, synapse maturation and subsequent formation of neural networks. Interestingly, recent genetic analyses of the 22q13.3 deletion syndrome, which is characterized by global developmental delay, absent or severely delayed speech and hypotonia, have suggested that the haplo-insufficiency for Shank3 is probably the cause of the pathological state as the Shank3 gene is located on chromosome 22q13.3 (Bonaglia *et al.* 2001; Wilson *et al.* 2003). Thus, clinical studies may lead to elucidation of the particular function of Shank3 and clarification of the specific function of Shank3 may lead to novel strategies for the treatment of this syndrome.

Acknowledgements

We thank Dr Masayoshi Mishina for the GluR1 (GluRα1), GluR2 (GluRα2) and NR2B (GluRε2) cDNAs. This study was supported by a grant from the Ministry of Health, Labour and Welfare, Japan.

References

Bliss T. V. P. and Collingridge G. L. (1993) A synaptic model of memory: long-term potentiation in the hippocampus. *Nature* **361**, 31–39.

Böckers T. M., Mameza M. G., Kreutz M. R., Bockmann J., Weise C., Buck F., Richter D., Gundelfinger E. D. and Kreienkamp H.-J. (2001) Synaptic scaffolding proteins in rat brain. Ankyrin repeats of the multidomain Shank protein family interact with the cytoskeletal protein α-fodrin. *J. Biol. Chem.* **276**, 40 104–40 112.

Böckers T. M., Bockmann J., Kreutz M. R. and Gundelfinger E. D. (2002) ProSAP/Shank proteins – a family of higher order organizing molecules of the postsynaptic density with an emerging role in human neurological disease. *J. Neurochem.* **81**, 903–910.

Böckers T. M., Segger-Junius M., Iglauer P., Bockmann J., Gundelfinger E. D., Kreutz M. R., Richter D., Kindler S. and Kreienkamp H.-J. (2004) Differential expression and dendritic transcript localization of Shank family members: identification of a dendritic targeting element in the 3′ untranslated region of Shank1 mRNA. *Mol. Cell Neurosci.* **26**, 182–190.

Bonaglia M. C., Giorda R., Borgatti R., Felisari G., Gagliardi C., Selicorni A. and Zuffardi O. (2001) Disruption of the ProSAP2 gene in a t(12;22)(q24.1;q13.3) is associated with the 22q13.3 deletion syndrome. *Am. J. Hum. Genet.* **69**, 261–268.

Carlin R. K., Grab D. J., Cohen R. S. and Siekevitz P. (1980) Isolation and characterization of postsynaptic densities from various brain regions: enrichment of different types of postsynaptic densities. *J. Cell Biol.* **86**, 831–843.

Chomczynski P. and Sacchi N. (1987) Single-step method of RNA isolation by acid guanidinium thiocyanate-phenol-chloroform extraction. *Anal. Biochem.* **162**, 156–159.

Cohen N. A., Brenman J. E., Snyder S. H. and Bredt D. S. (1996) Binding of the inward rectifier K^+ channel Kir 2.3 to PSD-95 is regulated by protein kinase A phosphorylation. *Neuron* **17**, 759–767.

Durand G. M., Kovalchuk Y. and Konnerth A. (1996) Long-term potentiation and functional synapse induction in developing hippocampus. *Nature* **381**, 71–75.

Hayashi Y., Shi S.-H., Esteban J. A., Piccini A., Poncer J.-C. and Malinow R. (2000) Driving AMPA receptors into synapses by LTP and CaMKII: Requirement for GluR1 and PDZ domain interaction. *Science* **287**, 2262–2267.

Hirasawa T., Wada H., Kohsaka S. and Uchino S. (2003) Inhibition of NMDA receptors induces delayed neuronal maturation and sustained proliferation of progenitor cells during neocortical development. *J. Neurosci. Res.* **74**, 676–687.

Hollmann M. and Heinemann S. (1994) Cloned glutamate receptors. *Annu. Rev. Neurosci.* **17**, 31–108.

Im Y. J., Lee J. H., Park S. H., Park S. J., Rho S.-H., Kang G. B., Kim E. and Eom S. H. (2003) Crystal structure of the Shank PDZ-ligand complex reveals a class I PDZ interaction and a novel PDZ-PDZ dimerization. *J. Biol. Chem.* **278**, 48 099–48 104.

Isaac J. T. (2003) Postsynaptic silent synapses: evidence and mechanisms. *Neuropharmacology* **45**, 450–460.

Leonard A. S., Davare M. A., Horne M. C., Garner C. C. and Hell J. W. (1998) SAP97 is associated with the α-amino-3-hydroxy-5-methylisoxazole-4-propionic acid receptor GluR1 subunit. *J. Biol. Chem.* **273**, 19 518–19 524.

Liao D., Scannevin R. H. and Huganir R. (2001) Activation of silent synapses by rapid activity-dependent synaptic recruitment of AMPA receptors. *J. Neurosci.* **21**, 6008–60017.

Lim S., Naisbitt S., Yoon J., Hwang J.-I., Suh P.-G., Sheng M. and Kim E. (1999) Characterization of the shank family of synaptic proteins. Multiple genes, alternative splicing, and differential expression in brain and development. *J. Biol. Chem.* **274**, 29 510–29 518.

McDonald J. W. and Johnston M. V. (1990) Physiological and pathophysiological roles of excitatory amino acids during central nervous system development. *Brain Res. Brain Res. Rev.* **15**, 41–70.

Naisbitt S., Kim E., Tu J. C., Xiao B., Sala C., Valtschanoff J., Weinberg R. J., Worley P. F. and Sheng M. (1999) Shank, a novel family of postsynaptic density proteins that binds to the NMDA receptor/PSD-95/GKAP complex and cortactin. *Neuron* **23**, 569–582.

Pickard L., Noël J., Henley J. M., Collingridge G. L. and Molnar E. (2000) Developmental changes in synaptic AMPA and NMDA receptor distribution and AMPA receptor subunit composition in living hippocampal neurons. *J. Neurosci.* **20**, 7922–7931.

Roussignol G., Ango F., Romorini S., Tu J. C., Sala C., Worley P. F., Bockaert J. and Fagni L. (2005) Shank expression is sufficient to induce functional dendritic spine synapses in aspiny neurons. *J. Neurosci.* **25**, 3560–3570.

Sans N., Racca C., Petralia R. S., Wang Y.-X., McCallum J. and Wenthold R. J. (2001) Synapse-associated protein 97 selectively associates with a subset of AMPA receptors early in their biosynthetic pathway. *J. Neurosci.* **21**, 7506–7516.

Sheng M. and Kim E. (2000) The Shank family of scaffold proteins. *J. Cell Sci.* **113**, 1851–1856.

Shi S.-H., Hayashi Y., Petralia R. S., Zaman S. H., Wenthold R. J., Svoboda K. and Malinow R. (1999) Rapid spine delivery and redistribution of AMPA receptors after synaptic NMDA receptor activation. *Science* **284**, 1811–1816.

Shi S.-H., Hayashi Y., Esteban J. A. and Malinow R. (2001) Subunit-specific rules governing AMPA receptor trafficking to synapses in hippocampal pyramidal neurons. *Cell* **105**, 331–343.

Songyang Z., Fanning A. S., Fu C., Xu J., Marfatia S. M., Chishti A. H., Crompton A., Chan A. C., Anderson J. M. and Cantley L. C. (1997) Recognition of unique carboxyl-terminal motifs by distinct PDZ domains. *Science* **275**, 73–77.

Tu J. C., Xiao B., Naisbitt S. *et al.* (1999) Coupling of mGluR/Homer and PSD-95 complexes by the Shank family of postsynaptic density proteins. *Neuron* **23**, 583–592.

Valtschanoff J. G., Burette A., Davare M. A., Leonard A. S., Hell J. W. and Weinberg R. J. (2000) SAP97 concentrates at the postsynaptic density in cerebral cortex. *Eur. J. Neurosci.* **12**, 3605–3614.

Wilson H. L., Wong A. C., Shaw S. R., Tse W. Y., Stapleton G. A., Phelan M. C., Hu S., Marshall J. and McDermid H. E. (2003) Molecular characterization of the 22q13.3 deletion syndrome supports the role of haploinsufficiency of SHANK3/PROSAP2 in the major neurological symptoms. *J. Med. Genet.* **40**, 575–584.

Wisden W. and Seeburg P. H. (1993) Mammalian ionotropic glutamate receptors. *Curr. Opin. Neurobiol.* **3**, 291–298.

Wu G., Malinow R. and Cline H. T. (1996) Maturation of a central glutamatergic synapse. *Science* **274**, 972–976.

Zhu J. J., Esteban J. A., Hayashi Y. and Malinow R. (2000) Postnatal synaptic potentiation: delivery of GluR4-containing AMPA receptors by spontaneous activity. *Nat. Neurosci.* **3**, 1098–1106.

Available online at www.sciencedirect.com
ScienceDirect
Biochemical and Biophysical Research Communications 350 (2006) 82–90
BBRC
www.elsevier.com/locate/ybbrc

Monoubiquitylation of GGA3 by hVPS18 regulates its ubiquitin-binding ability

Satomi Yogosawa [a,b], Masato Kawasaki [c], Soichi Wakatsuki [c], Eiki Kominami [d], Yoko Shiba [e], Kazuhisa Nakayama [e], Shinichi Kohsaka [a,*], Chihiro Akazawa [a]

[a] *Department of Neurochemistry, National Institute of Neuroscience, NCNP, Kodaira, Tokyo 187-8502, Japan*
[b] *Division of Molecular Biology, Research Institute for Biological Sciences, Tokyo University of Science, Noda, Chiba 278-0022, Japan*
[c] *Structural Biology Research Center, Photon Factory, Institute of Materials Structure Science, High Energy Accelerator Research Organization (KEK), Tsukuba, Ibaraki 305-0801, Japan*
[d] *Department of Biochemistry, Juntendo University School of Medicine, Bunkyo-ku, Tokyo 113-8421, Japan*
[e] *Graduate School of Pharmaceutical Science, Kyoto University, Sakyo-ku, Kyoto 606-8501, Japan*

Received 25 August 2006
Available online 15 September 2006

Abstract

GGAs (Golgi-localizing, γ-adaptin ear domain homology, ADP-ribosylation factor (ARF)-binding proteins), constitute a family of monomeric adaptor proteins and are associated with protein trafficking from the *trans*-Golgi network to endosomes. Here, we show that GGA3 is monoubiquitylated by a RING-H2 type-ubiquitin ligase hVPS18 (human homologue of *vacuolar protein sorting* 18). By *in vitro* ubiquitylation assays, we have identified lysine 258 in the GAT domain as a major ubiquitylation site that resides adjacent to the ubiquitin-binding site. The ubiquitylation is abolished by a mutation in either the GAT domain or ubiquitin that disrupts the GAT-ubiquitin interaction, indicating that the ubiquitin binding is a prerequisite for the ubiquitylation. Furthermore, the GAT domain ubiquitylated by hVPS18 no longer binds to ubiquitin, indicating that ubiquitylation negatively regulates the ubiquitin-binding ability of the GAT domain. These results suggest that the ubiquitin binding and ubiquitylation of GGA3-GAT domain are mutually inseparable through a ubiquitin ligase activity of hVPS18.

Keywords: GGA; GAT-domain; hVPS18; RING-H2 domain; Ubiquitin ligase; Monoubiquitylation; Ubiquitin-binding

In eukaryotic cells, vesicular trafficking of proteins between intracellular compartments, such as the Golgi complex and the multivesicular body (MVB)/lysosome, plays an important role in cellular functions. GGAs (Golgi-localizing, γ-adaptin ear domain homology, ADP-ribosylation factor (ARF)-binding proteins) are a family of monomeric adaptor proteins that regulate delivery of clathrin-coated vesicles from the TGN to endosomes [1–3]. In mammals, there are three GGAs (GGA1, GGA2, and GGA3) that share four functional domains, named VHS (Vps27/Hrs/Stam), GAT (GGA and Tom1 (target of Myb 1)), hinge, and GAE (γ-adaptin ear) [4–7]. The N-terminal VHS domain directly binds to acidic cluster-dileucine motifs found in the cytoplasmic domains of transmembrane cargo proteins [8–10]. The GAT domain is responsible for association of GGAs with the TGN membrane through interacting with activated ARF (a GTP-bound form) [11]. The proline-rich hinge region, the most variable among the GGA isoforms, mediates recruitment of clathrin [12]. The C-terminal GAE domain associates with various accessory proteins that modulate vesicle transport [1,3].

In the past few years, a number of proteins that are involved in membrane trafficking, especially in endocytosis and degradation in lysosomes, have been shown to be

* Corresponding author. Fax: +81 42 346 1751.
E-mail address: kohsaka@ncnp.go.jp (S. Kohsaka).

0006-291X/$ - see front matter © 2006 Elsevier Inc. All rights reserved.
doi:10.1016/j.bbrc.2006.09.013

functionally modulated by their ubiquitin binding and ubiquitylation [13–16]. Recently, it has also been shown that ubiquitin binding and ubiquitylation play an important role in selective transport of proteins from the TGN. The GAT domains of GGAs bind to ubiquitin and/or ubiquitylated proteins and undergo monoubiquitylation in the cell [17–20]. The interaction between the GAT domain and ubiquitin may endow GGAs with the ability to sort ubiquitylated transmembrane proteins at both the TGN and endosomes. Several ubiquitin ligases (E3) have been shown to be involved in monoubiquitylation of membrane-associated proteins and to participate in the endocytic and degradation pathways [21]. For example, c-Cbl, a RING-type ligase, ubiquitylates epidermal growth factor receptor (EGFR) depending on ligand-stimulated phosphorylation of the receptor [22], and Nedd4, a HECT-type ligase, is required for monoubiquitylation of eps15 and Hrs [23,24].

The Class C Vps (vacuolar protein sorting) complex is required for vesicle transport from the late endosome to vacuole in yeast [25,26]. In mammals, VPS proteins also appear to control the fusion events of late endosomes and lysosomes [27,28]. In humans, four Class C VPS proteins, hVPS11, hVPS16, hVPS18, and hVPS33, constitute a large hetero-oligomeric complex that interacts with syntaxin 7 at late endosomes/lysosomes [29]. Moreover, they also exist as a large detergent-insoluble HOPS (homotypic fusion and vacuole protein sorting) complex that contains additional components, hVPS39/Vam6, and hVPS41/Vam2 [27]. Overexpression of VPS39/Vam6S alters the late endosome function in mammalian cells [30]. Thus, it is necessary to discuss specific functions of Class C VPS proteins based on the biochemical properties.

In this report, we have demonstrated that GGAs (GGA1 and GGA3 but not GGA2) are monoubiquitylated by hVPS18, a RING-H2 type ubiquitin ligase, and identified a lysine residue in the C-terminal subdomain of the GAT domain as a major ubiquitylation site. Furthermore, we have shown that the monoubiquitylation negatively regulates the ubiquitin-binding ability of GGA itself. These observations shed light on the regulatory mechanisms of GGA to participate in membrane trafficking through the association of hVPS18.

Materials and methods

Plasmid construction. Full-length and various truncated human GGA cDNAs, as described previous, [17], were subcloned into the following vector: the pGEX-4T2 (Amersham Biosciences) prokaryotic expression vector for the production of GST-tagged fusion proteins. Myc-tagged hVPS18 and hVPS11 mammalian expression vectors were prepared as described previously [29]. The full-length hVPS18, hVPS11, and hVPS16 were subcloned into pFastBacHTb insect expression vector (Invitrogen) to generate His_6-tagged fusion proteins.

Expression and preparation of recombinant proteins. E2 ubiquitin-conjugating enzyme, human Ubc4, was produced in *Escherichia coli* strain BL21-AI (Invitrogen). GST-GGA (wild-type and truncated mutants) and GST-ubiquitin (Ub) (wild-type and mutants) were expressed in *E. coli* strain BL21-AI and the recombinant proteins were purified by using glutathione–Sepharose 4B beads (Amersham Biosciences) in PBS containing 1 mM PMSF, Complete protease inhibitor mixture, and 1% Triton X-100. His_6-tagged hVPS18, hVPS11, and hVPS16 were expressed in Sf-9 insect cells using baculovirus protein expression system (Invitrogen) and the recombinant proteins were purified under the denatured condition (8 M urea), and followed by using TALON metal affinity beads (BD Biosciences), and renatured in PBS. Circular dichroism spectra of the wild-type and mutant proteins were recorded on a Jasco J-820 spectropolarimeter at 25 °C using a cuvette with 1 mm path length with the protein concentration of 30 μM in PBS.

Antibody. Polyclonal antibody against human GGA1, GGA2, and GGA3 was raised in rats by immunization with purified full-length GGA1, GGA2, and GGA3, respectively. These antibodies were affinity-purified on HiTrap NHS-activated columns (Amersham Biosciences) conjugated with immunogens. Monoclonal GGA3 antibody was purchased from BD Transduction Laboratories. Anti-hVPS18, hVPS11, and hVPS16 antibodies were prepared as described previously [29].

Immunocytochemistry. HeLa cells were immunostained with mouse anti-GGA3 antibody and rabbit anti-hVPS18 as described previously [29]. To confirm intracellular colocalization, immunoreactivities were analyzed by the sectioning microscope (Delta Vision) calibrated by using fluorescent beads (TetraSpeck Fluorescent Microsphere Standards, 0.1 μm, Invitrogen).

Immunoprecipitation. Immunoprecipitation was performed as described previously [29]. Briefly, the cells were transfected with various plasmids by Fugene 6 reagent (Roche Molecular Biochemicals) according to the manufacturer's instructions. At 24 h after transfection, total cell lysates were incubated with 4 μg of anti-FLAG antibodies (monoclonal M2, Sigma) at 4 °C overnight. Immunoprecipitation of the antigen-antibody complex was accomplished by adding 40 μl of protein G–Sepharose for 1 h at 4 °C. Sepharose bound proteins were subjected to SDS–PAGE and detected by Western blot analyses with anti-Myc antibody (Roche Molecular Biochemicals) or anti-FLAG M2 antibody, respectively.

In vitro pull-down assay. In vitro pull-down assay was performed as described previously [31]. Briefly, GST-GGA-GAT proteins were immobilized on glutathione–Sepharose 4B beads and incubated with His_6-hVPS18 at 25 °C for 30 min. The resin was washed, subjected to SDS–PAGE, and detected by Western blot analyses with either anti-His_6 antibody (Santa Cruz Biotechnology) or anti-GST antibody.

We performed assays of GGA3 binding to ubiquitin as described previous [17]. Briefly, various GGA3 proteins were incubated with Ub-(10 μl) or protein A–agarose (15 μl) beads (Sigma) for 1 h at room temperature. The beads were washed, subjected to SDS–PAGE, and detected by Western blot analyses using anti-GST antibody.

To prepare ubiquitylated GGA3 C-GAT proteins, GGA3 C-GAT proteins were subjected to *in vitro* ubiquitylation assay and immobilized on glutathione–Sepharose 4B beads. The beads were then washed with a buffer (25 mM Hepes, pH 7.4, 0.1% Nonidet P-40, 0.5 M NaCl, and 50% ethylene glycol) and eluted with 25 mM Hepes, pH 7.4, 20 mM reduced glutathione.

In vitro ubiquitylation assay. An *in vitro* ubiquitylation assay was performed as described previously [29]. Briefly, GST-GGA proteins were mixed with yeast E1 (500 ng) (Boston Biochem), human Ubc4, ubiquitin (Boston Biochem) or GST-Ub (10 or 5 μg, respectively), and His_6-tagged hVPS18 (or hVPS11 or hVPS16). The mixture was incubated at 25 °C for 30 or 60 min in the presence of 50 mM Tris–HCl, pH 7.4, 5 mM $MgCl_2$, 2 mM dithiothreitol (DTT), and 4 mM ATP in a 20 μl volume. After incubation, the mixtures were immobilized on glutathione–Sepharose 4B beads and washed with wash buffer for three times. The resin was subjected to SDS–PAGE and detected by Western blot analyses using anti-GST antibody or anti-His_6 antibody or specific antibody.

Results and discussion

Direct interaction with GGAs and hVPS18

Recent studies identified the GAT domain as a ubiquitin-binding module [17–20]. Furthermore, our recent yeast

two-hybrid screening using hVPS18 as bait identified a partial fragment of GGA3 [31]. We first confirmed the molecular interaction by an *in vitro* pull-down assay using recombinant GGAs and hVPS18. As shown in Fig. 1A, His_6-hVPS18 was pulled down with the GST fusion of the GAT domain of GGA1, GGA2 or GGA3. We next analyzed the *in vivo* interaction by a co-immunoprecipitation experiment using lysates of cells cotransfected with FLAG-GGAs and either Myc-hVPS18 or Myc-hVPS11. As shown in Fig. 1B, all GGAs co-immunoprecipitated hVPS18. By contrast, either GGA could not interact with hVPS11, another Class C component having a RING-H2

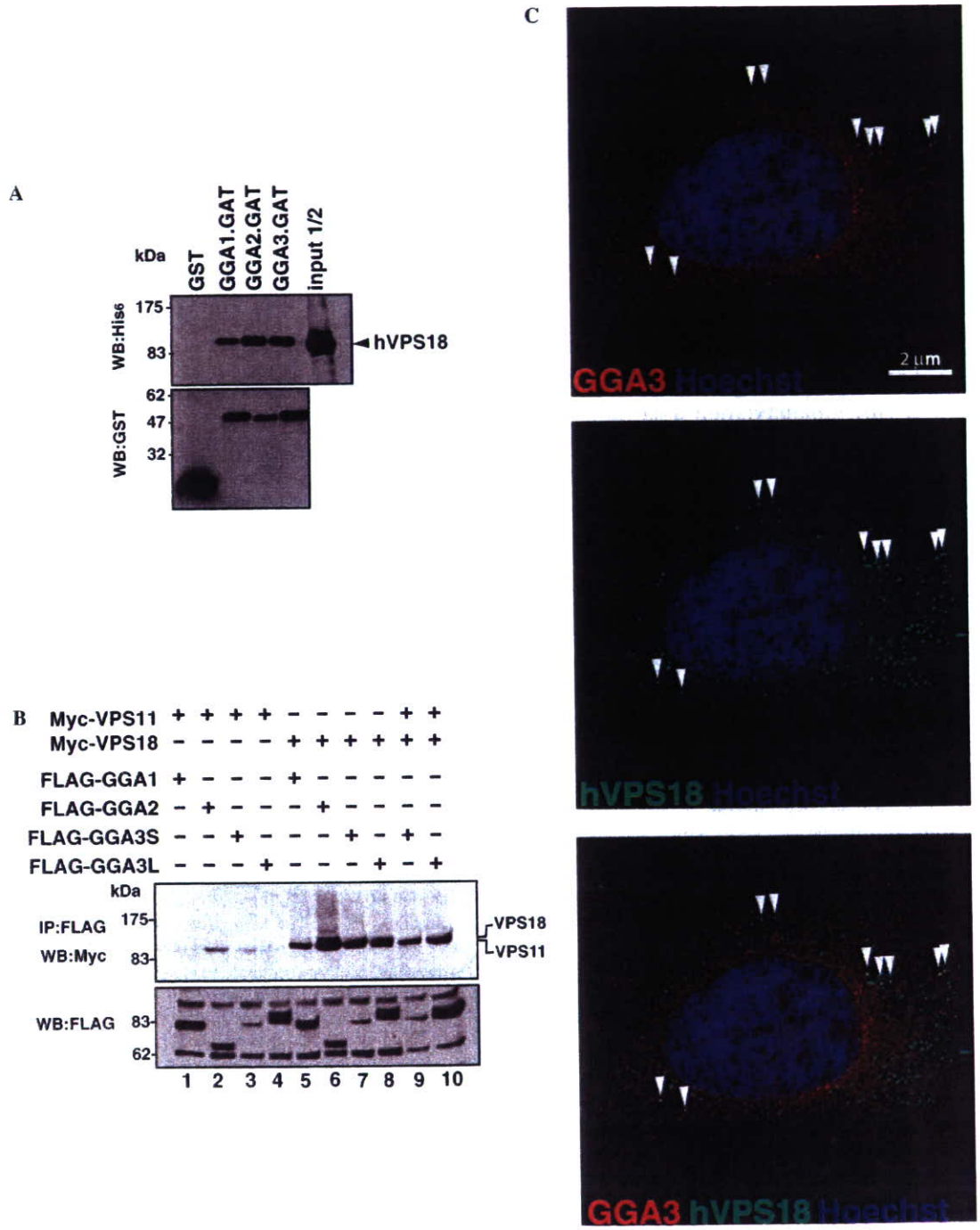

Fig. 1. GGA-GAT domains interact with hVPS18. (A) His_6-hVPS18 bound to three GST-GGA-GAT proteins was detected by Western blot analyses using anti-GST antibody. (B) Cos7 cells were co-transfected with His_6-FLAG-GGAs and Myc-hVPS11 or hVPS18. At 24 h post-transfection, whole-cell lysates were co-immunoprecipitated using anti-FLAG M2 antibody. Immunoprecipitates were resolved by SDS–PAGE and detected by Western blot analyses using indicated antibody. (C) The interaction of endogenous GGA3 (*Red*) and hVPS18 (*Green*) in HeLa cells was detected by immunocytochemistry. Colocalizing profiles are pointed out with *arrows*. *Bar*, 2 μm.

domain. Considering the molecular interaction between GGAs and hVPS18, a major issue that arises is the intracellular localization of these proteins. GGAs have been characterized as TGN-associated clathrin adaptors, whereas the Class C VPS complex has been proposed to function in endosomal/lysosomal compartments. We therefore analyzed the precise intracellular localization of endogenous GGA3 and hVPS18 in HeLa cells by the sectioning microscopy. The optical pathways were calibrated using fluorescent labeled beads (0.1 μm diameter). The thirty series of sections covering 5 μm thickness were captured and deconvoluted images were analyzed. As shown in a representative image Fig. 1C, GGA3 immunoreactivities (colored in *Red*) and hVPS18 immunoreactivities (colored in *Green*) were often colocalized on punctuates (colored in *Yellows*) of perinuclear structures (indicated by arrowheads).

Monoubiquitylation of GGAs by hVPS18, RING-H2 type ubiquitin ligase

Our recent study, showed that the RING-H2 domain of hVPS18 displays a E3 ubiquitin ligase activity [31]. To examine whether GGAs are ubiquitylated by the hVPS18, we performed an *in vitro* ubiquitylation assay using full-length GGAs as substrates. As shown in Fig. 2A, the molecular weight of GGA1 and GGA3 was shifted by ~8 kDa only in the simultaneous presence of ubiquitin, E1, E2 (UbcH4), and hVPS18 (lanes 2 and 6, respectively). By contrast, the shift was not observed in the case of GGA2 (lane 4), being compatible with our previous study showing that GGA2 is not able to interact with ubiquitin nor ubiquitylated in the cell. We next examined whether the *in vitro* modification represents monoubiquitylation/multiubiquitylation or not. In this experiment, we used wild-type (WT) ubiquitin fused to GST, and its K48R and KO (all lysine residues were replaced with arginine) mutants, since these mutants are not conjugated to conventional polyubiquitin chains. As shown in Fig. 2B, when GST-ubiquitin WT was used, the molecular weight of the GGA3-GAT domain was shifted by 35 kDa, which corresponds to the size of GST-ubiquitin. Essentially the same band shift was observed using the K48R and KO mutants, indicating that GGA3 is mainly monoubiquitylated by hVPS18.

Since hVPS18 forms a complex with other Class C VPS components [29], we then examined whether hVPS11 and hVPS16 were also involved in the monoubiquitylation of GGA3. Although hVPS11 also has a RING-H2 domain and shows a ubiquitin ligase activity (data not shown), it did not ubiquitylate the GGA3-VHS+GAT domain irrespective of the presence of hVPS16 (Fig. 2C lanes 2 and 3). However, the monoubiquitylation of GGA3 by hVPS18 was extremely enhanced in the presence of hVPS11 and hVPS16 (compare lane 5 with lanes 6 and 7). This result makes it likely that hVPS18 is involved in the monoubiquitylation of GGA3 as a Class C VPS complex.

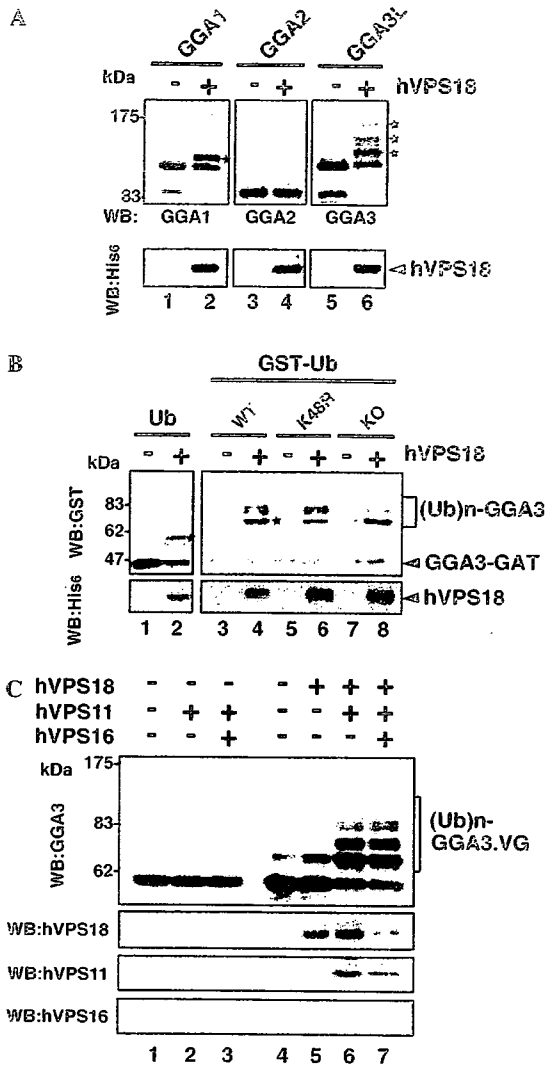

Fig. 2. GGAs are monoubiquitylated by hVPS18. (A) The *in vitro* ubiquitylation of GST-GGAs wild-type by His_6-hVPS18. The sample was detected by Western blot analyses using anti-GGA1, GGA2, or GGA3 (upper panel). Purified His_6-hVPS18 protein was detected by Western blot analyses using anti-His_6 antibody (lower panel). Asterisks represent ubiquitylated form of GGAs. (B) The *in vitro* ubiquitylation of GST-GGA3-GAT protein in the presence of no-tagged ubiquitin (Ub) or GST-fused ubiquitin (GST-Ub); wild-type (WT), K48R, or all lysines mutated to arginines (KO). The sample was detected by Western blot analyses using anti-GST or anti-His_6 antibody. Asterisks represent ubiquitylated forms of GGA3 that conjugate to Ub (left panel) or GST-Ub (right panel). (C) The *in vitro* ubiquitylation of GST-GGA3-VG (VHS+GAT) by hVPS11 or hVPS18 in the presence or absence of hVPS16. Purified His_6-tagged hVPS18 (or hVPS11 or hVPS16) protein was detected by Western blot analyses using specific antibodies.

Ubiquitin binding-dependent monoubiquitylation of GGA3-GAT

Identification of the ubiquitylation site is of great significance to discuss the molecular mechanism underlying the GGA ubiquitylation. We have recently shown that GGA3 is ubiquitylated in the C-terminal subdomain of its GAT domain (C-GAT) *in vivo* [17]. We therefore,

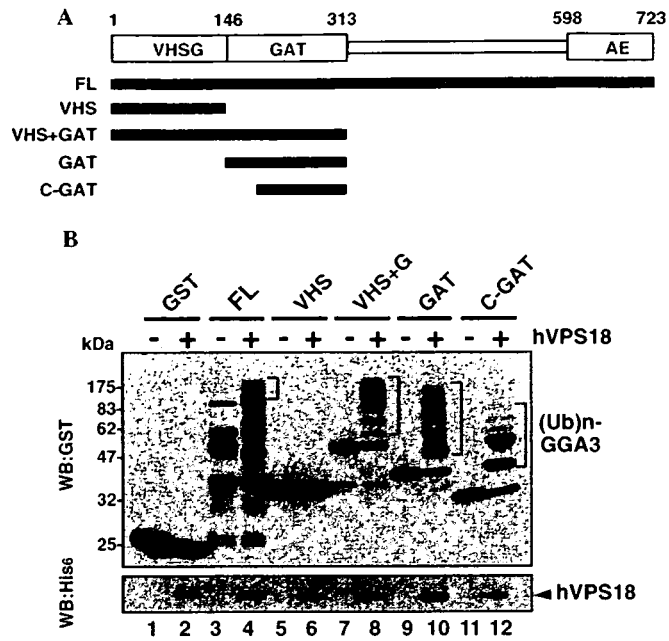

Fig. 3. GGA3 is ubiquitylated in the C-GAT domain. (A) Schematic representation of GGA3. (B) The *in vitro* ubiquitylation of GST-GGA3 full-length or truncated mutants. The sample was detected by Western blot analyses using anti-GST or anti-His_6 antibody. The positions of ubiquitylated GGA3 are indicated by a bracket.

performed an *in vitro* ubiquitylation assay using various truncation mutants of GGA3 (Fig. 3A). As shown in Fig. 3B, ubiquitylation occurred in the GGA3 fragments covering the C-GAT subdomain (lanes 4, 8, 10, and 12) but not in the GST protein (lane 2) nor the VHS domain alone (lane 6), in agreement with our previous ubiquitylation data in the cell [17].

Recent studies have shown, that many proteins containing ubiquitin-binding modules undergo monoubiquitylation and more importantly, their ubiquitin-binding ability is required for their own monoubuquitylation [23,32,33]. Therefore, we tested *in vitro* whether various GGA3 mutants that lack ubiquitin-binding ability were monoubiquitylated by hVPS18. As shown in Supplementary Fig. 1, the GGA3-GAT helix α3 mutant (L280R or D284G) defective in ubiquitin binding was not monoubiquitylated (compare lane 2 with lanes 6 and 8). Essentially the same result was obtained with a GGA3-GAT helix α2/α3 double mutant, E250N/D284G. These results indicate that binding to ubiquitin is a prerequisite for the GGA3 ubiquitylation. Next we constructed various truncated mutants of the GGA3-GAT domain (Supplementary Fig. 2A) and compared their ubiquitin binding (in Supplementary Fig. 2B) and ubiquitylation by hVPS18 (Supplementary Fig. 2C). Remarkably, all of the GAT fragments that retained ubiquitin-binding ability were monoubiquitylated by hVPS18, whereas the fragments lacking the ability were not monoubiquitylated. These data indicate that binding to ubiquitin and ubiquitylation of the GAT domain are intimately coupled events.

Lys258 is the major ubiquitylation site

In the C-GAT subdomain of GGA3, there are six lysine residues that can be conjugated to ubiquitin. To determine which lysine residue(s) was ubiquitylated, we systematically replaced the lysine residues with arginines (Fig. 4A) and examined binding to ubiquitin and monoubiquitylation of these lysine mutants. As shown in Fig. 4B, all of the C-GAT mutants examined retained their ubiquitin-binding ability. In striking contrast, they were variable in the ubiquitylation efficiency (Fig. 4C). Namely, (i) a mutant, 5KR(258), in which all the lysine residues except for K258 were replaced with arginines (Fig. 4A), underwent monoubiquitylation (lane 10) at comparable efficiency to that of the WT C-GAT subdomain (lane 2); (ii) the 5KR(249), 5KR(264), and 5KR(294) mutants underwent ubiquitylation at extremely low efficiency (lanes 8, 12, and 14); and (iii) ubiquitylation of 5KR(210), 5KR(213), and 6KR mutants was under the detection level (lanes 4, 6, and 16). As shown in Supplemental Figure 4, the circular dichroism spectra of WT and 5KR(258) were almost identical, suggesting that the mutations did not significantly affect the overall conformation of the C-GAT subdomain. Taken together, we conclude that lysine 258 is the major site ubiquitylated by hVPS18, although other lysine residues at positions 249, 264, and 294 were also ubiquitylated to some extent.

Model of GGA3-GAT domain ubiquitylated at Lys258

Previously, we determined the crystal structure of the complex between GGA3 C-GAT and ubiquitin, and showed primarily hydrophobic interactions in which the site 1 in C-CAT constitutes the binding site with three times higher affinity than the site 2 [34]. To understand the molecular basis for the coupling of ubiquitin binding and ubiquitylation of the GGA3-GAT domain, we mapped the positions of lysine residues of GGA3 C-GAT in the complex structure (Fig. 5). Among the six candidate lysine residues, lysine 258 is the closest to the C-terminus of ubiquitin (Fig. 5, Table 1), suggesting that this lysine is most susceptible to ubiquitin conjugation. This model also suggests that no major structural rearrangement between ubiquitin and the GGA3 C-GAT domain is required for the ubiquitylation of lysine 258.

Ubiquitylated GGA3 C-GAT loses its ubiquitin-binding ability

Hicke et al. have proposed a possibility that ubiquitylation of ubiquitin-binding proteins might generally have a regulatory function by affecting association of their ubiquitin-binding modules with either free ubiquitin or ubiquitylated proteins [13]. To address this possibility, we performed *in vitro* pull-down assay using reaction products of the *in vitro* ubiquitylation, in which both ubiquitylated and non-ubiquitylated C-GAT proteins were included. As

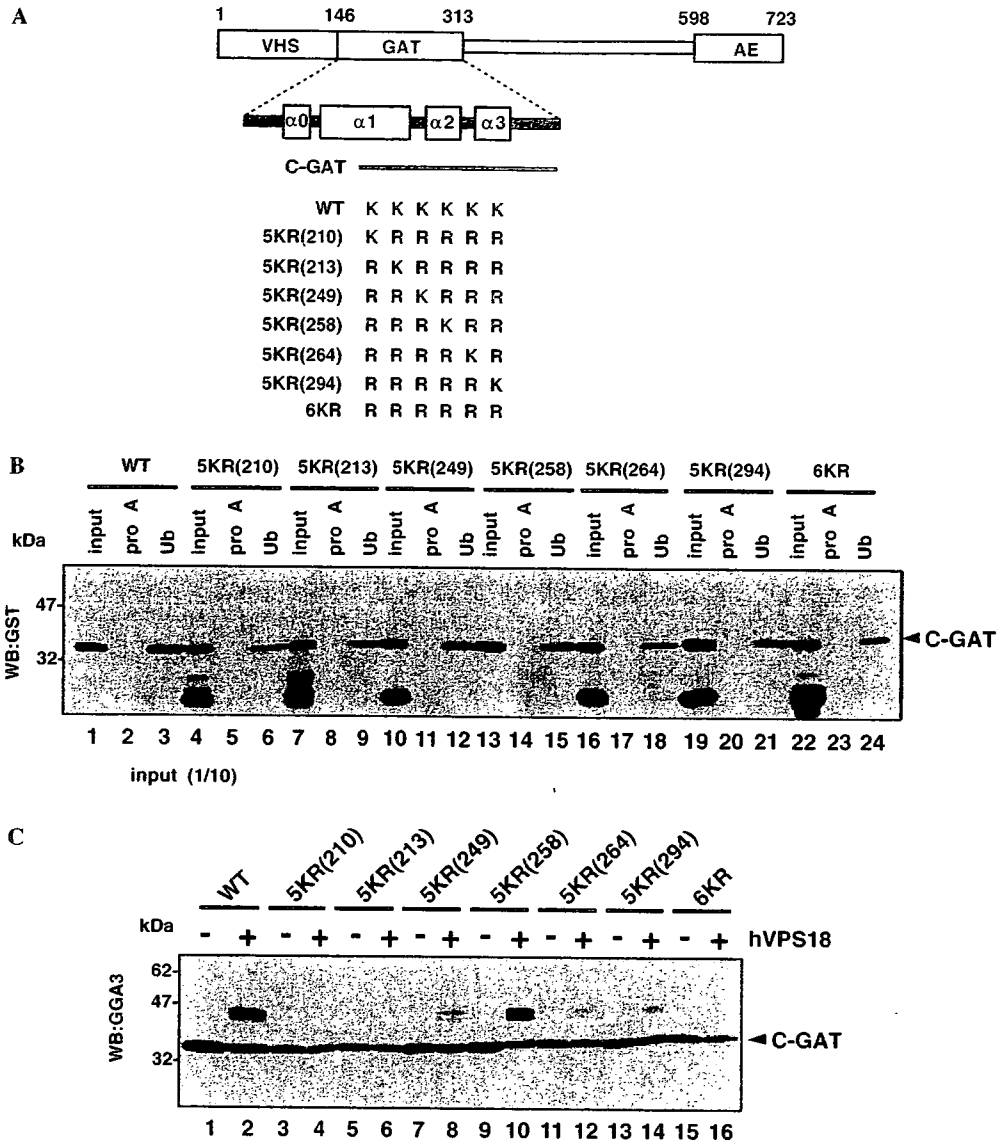

Fig. 4. GGA3 is mainly ubiquitylated at lysine 258 that resides in the two ubiquitin-binding sites. (A) Schematic representation of GGA3-GAT. (B) The *in vitro* pull-down assay of GGA3 C-GAT. Equal amounts of purified GGA3 C-GAT proteins were incubated with Ub- or Protein-A–agarose. The resin was washed, subjected to SDS–PAGE, and detected by Western blot analyses with anti-GST antibody. Ten percent of input samples were loaded on *input lanes*. (C) The *in vitro* ubiquitylation of GST-GGA3 C-GAT proteins. The sample was detected by Western blot analyses using anti-GGA3 antibody.

shown in Fig. 6, the ubiquitylated form of C-GAT WT or its 5KR(258) mutant was not pulled down with ubiquitin-agarose beads (lanes 3 and 7, indicated by asterisks), whereas their non-ubiquitylated forms were pulled down well. This result indicates that covalent modification by ubiquitin at lysine 258 makes C-GAT inaccessible to ubiquitin.

Recent advances have uncovered that several membrane-trafficking events are mediated by ubiquitin binding and monoubiquitylation, including changes in subcellular localization, protein conformation, activity, and protein-protein interaction. [16,35,36]. GGA might have evolved to allow a wide variety of proteins to interact directly with ubiquitin or ubiquitylated proteins during various cellular processes [1,20,37,38]. In this study, we first identified that hVPS18 acts as a genuine ubiquitin ligase of GGAs (Fig. 2A). The modification by hVPS18 slightly differs among GGAs; the monoubiquitylation occurs in one or multiple lysine sites of GGA1 and GGA3 but not of GGA2 (Figs. 2A and B). We then focused on GGA3 and tried to identify the responsible lysine. By taking an advantage of E3 identification, we utilized various KR mutants (Fig. 4). Finally, we identified the lysine 258 is the main target lysine for the ubiquitylation by hVPS18. If we closely look at the results of co-crystallization of GGA3 C-GAT and ubiquitin, the lysine 258 is located at the closest position to the C-terminus of ubiquitin, suggesting that the ubiquitin binding is necessary for ubiquitylation.

It has been recently shown that a free ubiquitin or ubiquitylated proteins are recognized by small (20–150 amino

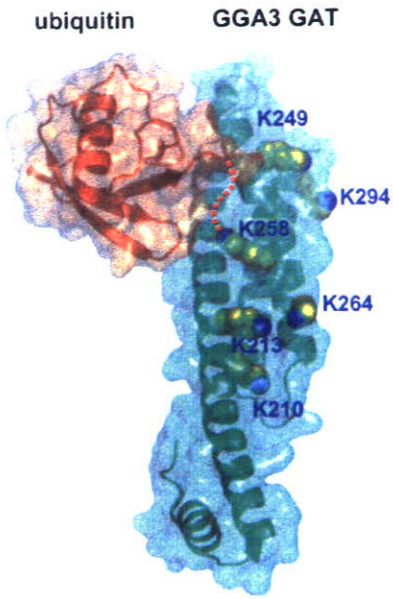

Fig. 5. Molecular surface representation of GGA3 C-GAT. The model was built by combining the crystal structures of the complex between ubiquitin and GGA3 C-GAT subdomain [34] and the entire GGA1 GAT domain [44]. Ubiquitin and GGA3 GAT domain are shown as ribbon diagrams with transparent surface representations (ubiquitin, *Orange*; GGA3 GAT, *Green*). Six lysine residues of the GGA3 C-GAT subdomain are shown with space-filling atoms (carbon atoms, *Yellow*; nitrogen atoms, blue). The C-terminal of ubiquitin (The last visible residue in the crystal, Leu73) and the side chain of Lys258 of GGA3 GAT are connected by an orange dotted line. Figure was drawn using PyMOL (http://pymol.sourceforge.net).

Table 1
Distances between the nitrogen atoms of the lysine side chains of C-GAT and the α carbon atom of Leu73 of ubiquitin, in the model structure in Fig. 5

Lysine	*210*	*213*	*249*	*258*	*264*	*294*
Distance (Å)	32.0	24.1	14.3	12.7	24.5	21.5

Leu73 of ubiquitin is the C-terminal residue visible in the crystal.

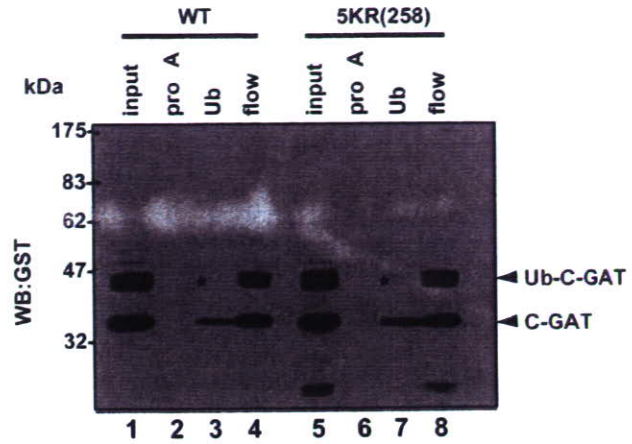

Fig. 6. Ubiquitylated GGA3 prevents further attachment to ubiquitin. The *in vitro* pull-down assay of ubiquitylated GGA3-GAT proteins. Equal amounts of ubiquitylated GGA3-GAT proteins were incubated with Ub- or Protein-A–agarose. The resin was washed, subjected to SDS–PAGE, and detected by Western blot analyses with anti-GST antibody. The supernatants were subjected to incubate with glutathione–Sepharose 4B (lanes 4 and 8). The 25% of input samples were loaded on *input lanes* (lane 1 and 5). Asterisks indicate that ubiquitylated forms of GGA3-GAT could not bind to Ub-agarose.

acids), independently folded motifs; ubiquitin-interacting motif (UIM), ubiquitin-associated (UBA), ubiquitin-conjugating enzyme-like (UBC)/ubiquitin E2 variant (UEV), or Cue1-homologous (CUE) domains [39]. These domains are also referred to as ubiquitin receptors [40]. However, in most cases, little is understood how biochemical interactions are transferred to downstream signals by these ubiquitin-binding proteins. Immediately after ubiquitin-binding abilities were reported, it was generally accepted that ubiquitin receptors are themselves ubiquitylated. Interestingly, the ubiquitylation of ubiquitin receptors requires ubiquitin binding. From our results, all of the GAT mutants that lack ubiquitin binding also inhibit ubiquitylation (Fig. 6). Conversely, a ubiquitin mutant (Ile44Ala) that cannot bind ubiquitin receptors per se cannot be conjugated to GAT domain. Previous reports described that the GAT domain contains two binding sites for ubiquitin [34]. The site 1 centers on leucine 227 and the site 2 centers on leucine 276. The site 1 has a higher affinity for ubiquitin than does site 2. When a ubiquitin was conjugated to the lysine 258 that is close to the site 1, no more ubiquitin can bind to the GGA3 C-GAT. This type of autoinhibition is reminiscent of intramolecular SH2-domain-phosphotyrosine interaction [41]. There has been a strong link between the presence of ubiquitin binding in a protein and its ubiquitylation. Ubiquitin binding and ubiquitylation of ubiquitin receptors are closely coupled and mutually inseparable [42,43]. But so far no ubiquitylation of lysine in the UBD has been reported. This is the first example demonstrating the ubiquitylated lysine resides in the UBD and consequently inhibit further ubiquitin binding. hVPS18 is one of the responsible E3 ubiquitin ligases that directly regulate the ubiquitin binding by conjugating ubiquitin in UBD of GGA3. A major question that has not been answered is to test how E3 hVPS18 is recruited to ubiquitin-binding proteins.

The ubiquitin ligase E3 functions as a monomer or a complex with other cofactors, such as SCF (Skp1/cullin/F-box protein) and the anaphase-promoting complex or cyclosome (APC/C) [35]. But none of the ligase activity has been observed when the catalytic subunit was solely added. Our study showed hVPS18, in the presence of E1 and E2, is sufficient for the *in vitro* ubiquitylation of GGA3, but the modification was significantly enhanced when equal molar of hVPS11 and hVPS16 are mixed. Previous report demonstrated that hVPS18, hVPS11, and hVPS16 constitute a hetero-oligomeric complex in the cytosolic membrane of endosome/lysosome [29]. The aug-

mented ligase-activity implies that the complex formation plays the functionally significant role both *in vivo* and *in vitro*.

In this report, we identified hVPS18 as a ubiquitin ligase (E3) for the monoubiquitylation of GGAs through their ability of ubiquitin-interaction. A number of molecules have been reported to interact with GGA, such as ARF, Rabaptin-5, clathrin, AP-1, and γ-synergin [1,3]. It will be a next issue to address whether these interactions are regulated via monoubiquitylation by hVPS18.

Appendix A. Supplementary data

Supplementary data associated with this article can be found, in the online version, at doi:10.1016/j.bbrc.2006.09.013.

References

[1] J.S. Bonifacino, The GGA proteins: adaptors on the move, Nat. Rev. Mol. Cell. Biol. 5 (2004) 23–32.
[2] I. Hinners, S.A. Tooze, Changing directions: clathrin-mediated transport between the Golgi and endosomes, J. Cell Sci. 116 (2003) 763–771.
[3] K. Nakayama, S. Wakatsuki, The structure and function of GGAs, the traffic controllers at the TGN sorting crossroads, Cell Struct. Funct. 28 (2003) 431–442.
[4] E.C. Dell'Angelica, R. Puertollano, C. Mullins, R.C. Aguilar, J.D. Vargas, L.M. Hartnell, J.S. Bonifacino, GGAs: a family of ADP ribosylation factor-binding proteins related to adaptors and associated with the Golgi complex, J. Cell Biol. 149 (2000) 81–94.
[5] H. Takatsu, K. Yoshino, K. Nakayama, Adaptor gamma ear homology domain conserved in gamma-adaptin and GGA proteins that interact with gamma-synergin, Biochem. Biophys. Res. Commun. 271 (2000) 719–725.
[6] J. Hirst, W.W. Lui, N.A. Bright, N. Totty, M.N. Seaman, M.S. Robinson, A family of proteins with gamma-adaptin and VHS domains that facilitate trafficking between the trans-Golgi network and the vacuole/lysosome, J. Cell Biol. 149 (2000) 67–80.
[7] M. Kawasaki, K. Nakayama, S. Wakatsuki, Membrane recruitment of effector proteins by Arf and Rab GTPases, Curr. Opin. Struct. Biol. (2005).
[8] R. Puertollano, R.C. Aguilar, I. Gorshkova, R.J. Crouch, J.S. Bonifacino, Sorting of mannose 6-phosphate receptors mediated by the GGAs, Science 292 (2001) 1712–1716.
[9] Y. Zhu, B. Doray, A. Poussu, V.P. Lehto, S. Kornfeld, Binding of GGA2 to the lysosomal enzyme sorting motif of the mannose 6-phosphate receptor, Science 292 (2001) 1716–1718.
[10] H. Takatsu, Y. Katoh, Y. Shiba, K. Nakayama, Golgi-localizing, gamma-adaptin ear homology domain, ADP-ribosylation factor-binding (GGA) proteins interact with acidic dileucine sequences within the cytoplasmic domains of sorting receptors through their Vps27p/Hrs/STAM (VHS) domains, J. Biol. Chem. 276 (2001) 28541–28545.
[11] H. Takatsu, K. Yoshino, K. Toda, K. Nakayama, GGA proteins associate with Golgi membranes through interaction between their GGAH domains and ADP-ribosylation factors, Biochem. J. 365 (2002) 369–378.
[12] R. Puertollano, P.A. Randazzo, J.F. Presley, L.M. Hartnell, J.S. Bonifacino, The GGAs promote ARF-dependent recruitment of clathrin to the TGN, Cell 105 (2001) 93–102.
[13] L. Hicke, H.L. Schubert, C.P. Hill, Ubiquitin-binding domains, Nat. Rev. Mol. Cell. Biol. 6 (2005) 610–621.
[14] M.D. Marmor, Y. Yarden, Role of protein ubiquitylation in regulating endocytosis of receptor tyrosine kinases, Oncogene 23 (2004) 2057–2070.
[15] P.P. Di Fiore, S. Polo, K. Hofmann, When ubiquitin meets ubiquitin receptors: a signalling connection, Nat. Rev. Mol. Cell. Biol. 4 (2003) 491–497.
[16] D.J. Katzmann, G. Odorizzi, S.D. Emr, Receptor downregulation and multivesicular-body sorting, Nat. Rev. Mol. Cell. Biol. 3 (2002) 893–905.
[17] Y. Shiba, Y. Katoh, T. Shiba, K. Yoshino, H. Takatsu, H. Kobayashi, H.W. Shin, S. Wakatsuki, K. Nakayama, GAT (GGA and Tom1) domain responsible for ubiquitin binding and ubiquitination, J. Biol. Chem. 279 (2004) 7105–7111.
[18] R. Puertollano, J.S. Bonifacino, Interactions of GGA3 with the ubiquitin sorting machinery, Nat. Cell Biol. 6 (2004) 244–251.
[19] P.M. Scott, P.S. Bilodeau, O. Zhdankina, S.C. Winistorfer, M.J. Hauglund, M.M. Allaman, W.R. Kearney, A.D. Robertson, A.L. Boman, R.C. Piper, GGA proteins bind ubiquitin to facilitate sorting at the trans-Golgi network, Nat. Cell Biol. 6 (2004) 252–259.
[20] R. Mattera, R. Puertollano, W.J. Smith, J.S. Bonifacino, The trihelical bundle subdomain of the GGA proteins interacts with multiple partners through overlapping but distinct sites, J. Biol. Chem. 279 (2004) 31409–31418.
[21] A. d'Azzo, A. Bongiovanni, T. Nastasi, E3 ubiquitin ligases as regulators of membrane protein trafficking and degradation, Traffic 6 (2005) 429–441.
[22] A.A. de Melker, G. van der Horst, J. Calafat, H. Jansen, J. Borst, c-Cbl ubiquitinates the EGF receptor at the plasma membrane and remains receptor associated throughout the endocytic route, J. Cell Sci. 114 (2001) 2167–2178.
[23] S. Polo, S. Sigismund, M. Faretta, M. Guidi, M.R. Capua, G. Bossi, H. Chen, P. De Camilli, P.P. Di Fiore, A single motif responsible for ubiquitin recognition and monoubiquitination in endocytic proteins, Nature 416 (2002) 451–455.
[24] M. Katz, K. Shtiegman, P. Tal-Or, L. Yakir, Y. Mosesson, D. Harari, Y. Machluf, H. Asao, T. Jovin, K. Sugamura, Y. Yarden, Ligand-independent degradation of epidermal growth factor receptor involves receptor ubiquitylation and Hgs, an adaptor whose ubiquitin-interacting motif targets ubiquitylation by Nedd4, Traffic 3 (2002) 740–751.
[25] T.K. Sato, P. Rehling, M.R. Peterson, S.D. Emr, Class C Vps protein complex regulates vacuolar SNARE pairing and is required for vesicle docking/fusion, Mol. Cell 6 (2000) 661–671.
[26] M.R. Peterson, S.D. Emr, The class C Vps complex functions at multiple stages of the vacuolar transport pathway, Traffic 2 (2001) 476–486.
[27] V. Poupon, A. Stewart, S.R. Gray, R.C. Piper, J.P. Luzio, The role of mVps18p in clustering, fusion, and intracellular localization of late endocytic prganelles, Mol. Bio. Cell 14 (2003) 4015–4027.
[28] S.C. Richardson, S.C. Winistorfer, V. Poupon, J.P. Luzio, R.C. Piper, Mammalian late vacuole protein sorting orthologues participate in early endosomal fusion and interact with the cytoskeleton, Mol. Biol. Cell 15 (2004) 1197–1210.
[29] B.Y. Kim, H. Kramer, A. Yamamoto, E. Kominami, S. Kohsaka, C. Akazawa, Molecular characterization of mammalian homologues of class C Vps proteins that interact with syntaxin-7, J. Biol. Chem. 276 (2001) 29393–29402.
[30] S. Caplan, L.M. Hartnell, R.C. Aguilar, N. Naslavsky, J.S. Bonifacino, Human Vam6p promotes lysosome clustering and fusion in vivo, J. Cell Biol. 154 (2001) 109–122.
[31] S. Yogosawa, S. Hatakeyama, K.I. Nakayama, H. Miyoshi, S. Kohsaka, C. Akazawa, Ubiquitylation and degradation of polo-like kinase SNK by hVPS18, a RING-H2 type ubiquitin ligase, J. Biol. Chem. 280 (2005) 41619–41627.
[32] S.L. Miller, E. Malotky, J.P. O'Bryan, Analysis of the role of ubiquitin-interacting motifs in ubiquitin binding and ubiquitylation, J. Biol. Chem. 279 (2004) 33528–33537.

[33] S.C. Shih, G. Prag, S.A. Francis, M.A. Sutanto, J.H. Hurley, L. Hicke, A ubiquitin-binding motif required for intramolecular monoubiquitylation, the CUE domain, EMBO J. 22 (2003) 1273–1281.
[34] M. Kawasaki, T. Shiba, Y. Shiba, Y. Yamaguchi, N. Matsugaki, N. Igarashi, M. Suzuki, R. Kato, K. Kato, K. Nakayama, S. Wakatsuki, Molecular mechanism of ubiquitin recognition by GGA3 GAT domain, Genes Cells 10 (2005) 639–654.
[35] A.M. Weissman, Themes and variations on ubiquitylation, Nat. Rev. Mol. Cell. Biol. 2 (2001) 169–178.
[36] R.C. Aguilar, B. Wendland, Ubiquitin: not just for proteasomes anymore, Curr. Opin. Cell Biol. 15 (2003) 184–190.
[37] Y. Katoh, Y. Shiba, H. Mitsuhashi, Y. Yanagida, H. Takatsu, K. Nakayama, Tollip and Tom1 form a complex and recruit ubiquitin-conjugated proteins onto early endosomes, J. Biol. Chem. 279 (2004) 24435–24443.
[38] M. Yamakami, T. Yoshimori, H. Yokosawa, Tom1, a VHS domain-containing protein, interacts with tollip, ubiquitin, and clathrin, J. Biol. Chem. 278 (2003) 52865–52872.
[39] K. Haglund, I. Dikic, Ubiquitylation and cell signaling, EMBO J. 24 (2005) 3353–3359.
[40] K. Haglund, P.P. Di Fiore, I. Dikic, Distinct monoubiquitin signals in receptor endocytosis, Trends Biochem. Sci. 28 (2003) 598–603.
[41] J. Kuriyan, D. Cowburn, Modular peptide recognition domains in eukaryotic signaling, Annu. Rev. Biophys. Biomol. Struct. 26 (1997) 259–288.
[42] M. Bienko, C.M. Green, N. Crosetto, F. Rudolf, G. Zapart, B. Coull, P. Kannouche, G. Wider, M. Peter, A.R. Lehmann, K. Hofmann, I. Dikic, Ubiquitin-binding domains in Y-family polymerases regulate translesion synthesis, Science 310 (2005) 1821–1824.
[43] D. Hoeller, N. Crosetto, B. Blagoev, C. Raiborg, R. Tikkanen, S. Wagner, K. Kowanetz, R. Breitling, M. Mann, H. Stenmark, I. Dikic, Regulation of ubiquitin-binding proteins by monoubiquitination, Nat. Cell Biol. 8 (2006) 163–169.
[44] T. Shiba, M. Kawasaki, H. Takatsu, T. Nogi, N. Matsugaki, N. Igarashi, M. Suzuki, R. Kato, K. Nakayama, S. Wakatsuki, Molecular mechanism of membrane recruitment of GGA by ARF in lysosomal protein transport, Nat. Struct. Biol. 10 (2003) 386–393.

American Journal of Pathology, Vol. 169, No. 1, July 2006

DOI: 10.2353/ajpath.2006.060085

Cell Injury, Repair, Aging and Apoptosis

Photoreceptor Cell Apoptosis in the Retinal Degeneration of *Uchl3*-Deficient Mice

Yae Sano,*† Akiko Furuta,* Rieko Setsuie,*† Hisae Kikuchi,* Yu-Lai Wang,* Mikako Sakurai,*† Jungkee Kwon,*‡ Mami Noda,† and Keiji Wada*

From the Department of Degenerative Neurological Diseases, National Institute of Neuroscience, National Center of Neurology and Psychiatry, Tokyo, Japan; the Laboratory of Pathophysiology,† Graduate School of Pharmaceutical Sciences, Kyushu University, Fukuoka, Japan; and the Laboratory of Animal Medicine,‡ College of Veterinary Medicine, Chonbuk National University, Jeonju, Korea*

UCH-L3 belongs to the ubiquitin C-terminal hydrolase family that deubiquitinates ubiquitin-protein conjugates in the ubiquitin-proteasome system. A murine *Uchl3* deletion mutant displays retinal degeneration, muscular degeneration, and mild growth retardation. To elucidate the function of UCH-L3, we investigated histopathological changes and expression of apoptosis- and oxidative stress-related proteins during retinal degeneration. In the normal retina, UCH-L3 was enriched in the photoreceptor inner segment that contains abundant mitochondria. Although the retina of *Uchl3*-deficient mice showed no significant morphological abnormalities during retinal development, prominent retinal degeneration became manifested after 3 weeks of age associated with photoreceptor cell apoptosis. Ultrastructurally, a decreased area of mitochondrial cristae and vacuolar changes were observed in the degenerated inner segment. Increased immunoreactivities for manganese superoxide dismutase, cytochrome *c* oxidase I, and apoptosis-inducing factor in the inner segment indicated mitochondrial oxidative stress. Expression of cytochrome c, caspase-1, and cleaved caspase-3 did not differ between wild-type and mutant mice; however, immunoreactivity for endonuclease G was found in the photoreceptor nuclei in the mutant retina. Hence, loss of UCH-L3 leads to mitochondrial oxidative stress-related photoreceptor cell apoptosis in a caspase-independent manner. Thus, *Uchl3*-deficient mice represent a model for adult-onset retinal degeneration associated with mitochondrial impairment. *(Am J Pathol 2006, 169:132–141; DOI: 10.2353/ajpath.2006.060085)*

The ubiquitin system has been implicated in numerous cellular processes, including protein quality control, cell cycle, cell proliferation, signal transduction, membrane protein internalization, and apoptosis.[1,2] Ubiquitin-dependent processes are regulated by ubiquitinating enzymes, E1, E2, and E3, and deubiquitinating enzymes such as ubiquitin-specific proteases and ubiquitin C-terminal hydrolases (UCHs).[1,3–5] To date, four isozymes of UCHs, UCH-L1, UCH-L3, UCH-L4, and UCH-L5, have been cloned in mouse or human.[6–8] UCH-L1, also known as PGP 9.5, has been well characterized among the isozymes. UCH-L1 is selectively localized to brains and testis/ovaries[7] and functions as a ubiquitin ligase in addition to a deubiquitinating enzyme.[9] Furthermore, two distinct mutations are linked to Parkinson's disease in human[10] and gracile axonal dystrophy (*gad*) in mice.[11] UCH-L3, on the other hand, displays 52% amino acid identity to UCH-L1.[12] Uchl3 mRNA is expressed throughout various tissues and is especially enriched in testis and thymus.[13] In addition to its ubiquitin hydrolase activity, *in vitro* studies indicate that UCH-L3 cleaves the C terminus of the ubiquitin-like protein Nedd-8.[14,15] Although UCH-L1 and UCH-L3 are suggested to function as reciprocal modulators of germ cell apoptosis in experimental cryptorchid testis,[16] the cellular localization and function of UCH-L3 remain unknown in other organs.

Recently, *Uchl3*-deficient mice were generated with a deletion of exons 3 to 7, which are essential for hydrolase

Supported by grants-in-aid for scientific research from the Japan Society for the Promotion of Science; for priority area research from the Ministry of Education, Culture, Sports, Science and Technology, Japan; Kyushu University Foundation for Scientific Research from the Ministry of Health, Labour and Welfare, Japan; and the program for Promotion of Fundamental Studies in Health Sciences from the National Institute of Biomedical Innovation, Japan.

Accepted for publication March 23, 2006.

Address reprint requests to Akiko Furuta, M.D., Ph.D., Department of Degenerative Neurological Diseases, National Institute of Neuroscience, National Center of Neurology and Psychiatry, 4-1-1, Ogawahigashi, Kodaira, Tokyo 187-8502, Japan. E-mail: afuruta@ncnp.go.jp.

activity.[13] These mutant mice display postnatal retinal and muscular degenerations as well as mild growth retardation.[17] Retinal development is morphologically normal, but progressive retinal degeneration is reported to be evident at 3 months after birth.[17] However, precise chronological changes and the mechanism of the retinal degeneration in *Uchl3*-deficient mice has not been studied.

Both the caspase-dependent pathway and the caspase-independent pathway have been proposed to be involved in the models of retinal degeneration, including model animals for retinitis pigmentosa (such as Royal College of Surgeons (RCS) rat and retinal degeneration (*rd*) mice),[18] retinal detachment,[19] light injury,[20,21] ischemic injury,[22] and age-related macular degeneration.[23] In the ubiquitin system, UCH-L1 is involved in ischemia-induced apoptosis in the inner retina.[24] The role of UCH-L3 in retinal degeneration, however, is unclear.

To elucidate the function of UCH-L3, we investigated the histopathological changes and protein expression with respect to apoptotic pathways in *Uchl3*-deficient mice. Our results show that UCH-L3 is mainly localized to the photoreceptor inner segment that contains abundant mitochondria in the normal retina. *Uchl3*-deficient mice displayed caspase-independent apoptosis during postnatal retinal degeneration associated with increased expression of the markers for mitochondrial oxidative stress at the inner segment. We propose a possible antiapoptotic role of UCH-L3 in photoreceptor cells.

Materials and Methods

Animals

We used age-matched *Uchl3*-deficient mice and wild-type mice, all of which were offspring male from 15 to 20 pairs of heterozygotes that had been backcrossed with C57BL/6J at postnatal ages of 0 days (P0), 10 days (P10), 3 weeks (3w), 6 weeks (6w), 8 weeks (8w), and 12 weeks (12w). The total number of wild-type and *Uchl3*-deficient mice examined in the present study was 79, of which 30 mice were used for Western blotting, 42 mice were used for hematoxylin and eosin staining, immunohistochemistry, and terminal deoxynucleotidyl transferase-mediated dUTP nick end labeling (TUNEL) assay, and 7 mice were used for electron microscopy. The mice were maintained at the National Institute of Neuroscience, National Center of Neurology and Psychiatry (Tokyo, Japan). The experiments using the mice were approved by the Institute's Animal Investigation Committee.

Western Blotting

Eyes from P10-, 3w-, and 6w-old mice of both genotypes (10 mice in each time point, for a total of 30 mice) were lysed in protein lysis buffer (100 mmol/L Tris-HCl, pH 8.0, 300 mmol/L NaCl, 2% Triton X-100, 0.2% SDS, 2% sodium deoxycholate, 2 mmol/L EDTA) containing protease inhibitor (Complete protease inhibitor cocktail; Sigma-Aldrich, St. Louis, MO). The amount of total protein of each sample was determined by the Bio-Rad protein assay (Bio-Rad, Hercules, CA) using bovine serum albumin as a standard. Total protein (50 μg/lane) was separated by 15% SDS-polyacrylamide gels (Perfect NT Gel, DRC, Tokyo, Japan). Proteins were transferred to immuno-Blot polyvinylidene difluoride membranes (Bio-Rad) and incubated with 5% skim milk in TBST (50 mmol/L Tris-HCl-buffered saline, pH 7.0, containing 0.05% Triton X-100) for 1 hour at room temperature. The membranes were incubated with a 1:1000 dilution of each primary antibody for UCH-L1, UCH-L3,[25] and β-actin (1:1000; Sigma-Aldrich) overnight at 4°C. For the preparation of anti-mouse UCH-L1 antibody, histidine-tagged mouse UCH-L1 (6His-mUCH-L1) was prepared as described previously[26] and used to generate a polyclonal antiserum in rabbit (Takara, Tokushima, Japan). The polyclonal antibody was purified by affinity chromatography. The specificity of this antibody to the mouse UCH-L1 was verified by Western blotting using brain lysates from *gad* mice and wild-type mice (data not shown). The membranes were washed in TBST and further incubated with antimouse or rabbit IgG-horseradish peroxidase conjugate (1:1000; Chemicon, Temecula, CA). After washing in TBST, the membranes were developed with the Super Signal West Dura or Femto Extended Duration Substrate (Pierce, Rockford, IL) and analyzed with a ChemiImager (Alpha Innotech, San Leandro, CA). Western blotting was performed five times per each antibody.

Morphometric Analysis and Immunohistochemistry of Retina

Mice of both genotypes at P0, P10, 3w, 6w, 8w, and 12w of age (7 mice in each time point, total of 42 mice) were deeply anesthetized with diethylether, decapitated, and the eyes removed, immersion-fixed with 4% paraformaldehyde overnight at 4°C, and embedded in paraffin wax. Deparaffinized sections were stained with hematoxylin and eosin and examined under an Axioplan2 microscope (Carl Zeiss, Oberkochen, Germany) at a magnification ×400, and the thickness of each layer was measured using WinRoof software (Mitani Shoji, Tokyo, Japan).

For immunohistochemical studies, 5-μm-thick sagittal sections at the level of the optic nerve were deparaffinized and treated with 1% hydrogen peroxide (H_2O_2) for 30 minutes, incubated with 1% skim milk in phosphate-buffered saline (PBS, pH 7.4) for 1 hour at room temperature followed by incubation overnight at 4°C with each primary antibody for UCH-L1 and UCH-L3[25] diluted 1:500 in 1% skim milk in PBS. To characterize apoptosis- and oxidative stress-related proteins, antibodies to the following proteins were used; apoptosis-inducing factor (AIF; 1:500, Chemicon), caspase-1 (1:100; Cell Signaling Technology, Beverly, MA), caspase-3 (1:1000; Cell Signaling Technology), cleaved caspase-3 (1:50; Cell Signaling Technology), cytochrome *c* (1:1000; Santa Cruz Biotechnology, Santa Cruz, CA), cytochrome *c* oxidase I

(COX, 1:10,000; Molecular Probes, Eugene, OR), endonuclease G (Endo G; 1:500, Chemicon) and manganese superoxide dismutase (Mn-SOD; 1:10,000, Stressgen, Victoria, BC, Canada). The sections were washed in PBS and then incubated with biotinylated secondary antibodies diluted 1:500 in PBS containing 1% skim milk. The sections were treated with the VECTASTAIN Elite ABC kit (Vector Laboratories, Burlingame, CA) according to the manufacturer's protocol and developed with 0.02% 3,3′-diaminobenzidine tetrahydrochloride solution containing 0.003% H_2O_2. After visualization, sections were counterstained with hematoxylin. Sections were examined with an Axioplan2 microscope (Carl Zeiss). Immunohistochemistry was performed in at least three repeated experiments. The relative immunoreactivity for COX, Mn-SOD, AIF, and Endo G in each layer of mutant mice was compared with that of wild-type mice and was classified into no change (−), slight increase (±), mild increase (+), and marked increase (++).

TUNEL Staining

Apoptotic cells were examined in mice of both genotypes at P0, P10, 3w, 6w, 8w, and 12w (7 mice in each time point, for a total of 42 mice) by TUNEL stain using the Dead-End Fluorimetric TUNEL system kit (Promega, Madison, WI) according to the manufacturer's instructions. The sections were examined by using a confocal laser scanning microscope (Olympus, Tokyo, Japan). The microphotographs were captured at magnification ×400 (0.066 mm^2/each retinal section), positive cells were counted (Fluoview 2.0; Olympus), and the data were subjected to statistical analysis.

Electron Microscopic Analysis

3w-old mice of both genotypes (total 7 mice) were deeply anesthetized with 20% chloral hydrate aqueous solution and perfused with the following fixative: 2% paraformaldehyde, 2% glutaraldehyde in PBS, or sodium cacodylate buffer (pH 7.4). The eyes were removed and postfixed with the same fixative overnight at 4°C. The posterior segments of eyes were trimmed and washed with PBS or sodium cacodylate buffer, incubated in phosphate-buffered 1% osmium tetroxide for 1 hour, and dehydrated in ethanol and embedded in Epon 812 resin (TAAB, Berks, UK). Ultrathin sections (75 nm) were mounted on copper grids and stained with uranium acetate and lead citrate. The sections were observed using an H-7000 electron microscope (Hitachi, Tokyo, Japan). Morphometric analysis of mitochondria was performed by measuring average percentage of area occupied by cristae within a mitochondrion at the inner segment.

Statistical Analysis

In statistical analysis of thickness of retinal layers and TUNEL-positive cells, three wild-type and four *Uchl3*-deficient mice were used in each time point (P0, P10, 3w,

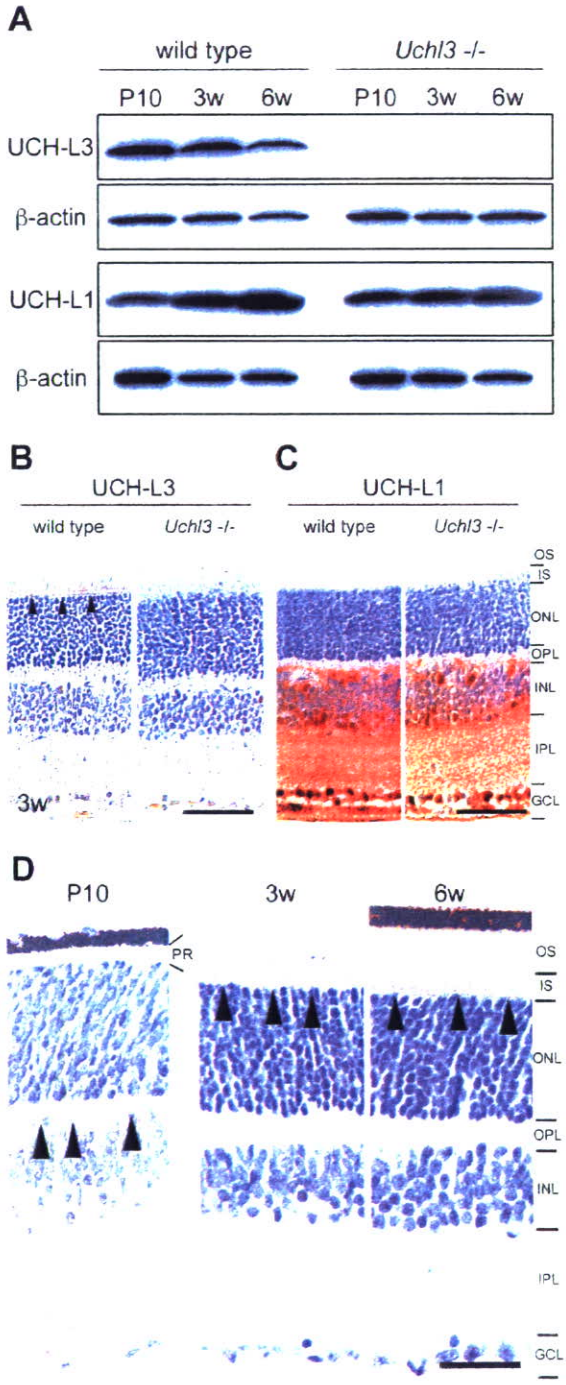

Figure 1. Expression of UCH-L1 and UCH-L3 in the retina of wild-type and *Uchl3*-deficient mice. **A:** Western blot analysis of UCH-L3 and UCH-L1 using whole-eye lysates from wild-type and *Uchl3*-deficient mice at P10, 3w, and 6w. The immunoreactive band for UCH-L3 is undetectable in *Uchl3*-deficient mice. Expression of UCH-L1 is similar between both genotypes. **B** and **C:** Immunohistochemistry for UCH-L3 (**B**) and UCH-L1 (**C**) in wild-type and *Uchl3*-deficient mice retinae at 3w. Immunoreactivity of UCH-L3 is found at the inner segment of the wild-type retina (**arrowheads**), whereas there is no significant immunoreactivity in *Uchl3*-deficient mice (**B**). UCH-L1 is expressed at the inner retina in both genotypes. **D:** Immunohistochemistry of UCH-L3 at P10, 3w, and 6w in wild-type retinae. UCH-L3 is faintly expressed in the outer plexiform layer at P10 (**arrowheads**). Thereafter, immunoreactivity for UCH-L3 is found in inner segment at 3w and 6w (**arrowheads**). PR, photoreceptor; OS, outer segment; IS, inner segment; ONL, outer nuclear layer; OPL, outer plexiform layer; INL, inner nuclear layer; IPL, inner plexiform layer; GCL, ganglion cell layer. Scale bars = 50 μm (**B** and **C**) and 20 μm (**D**).

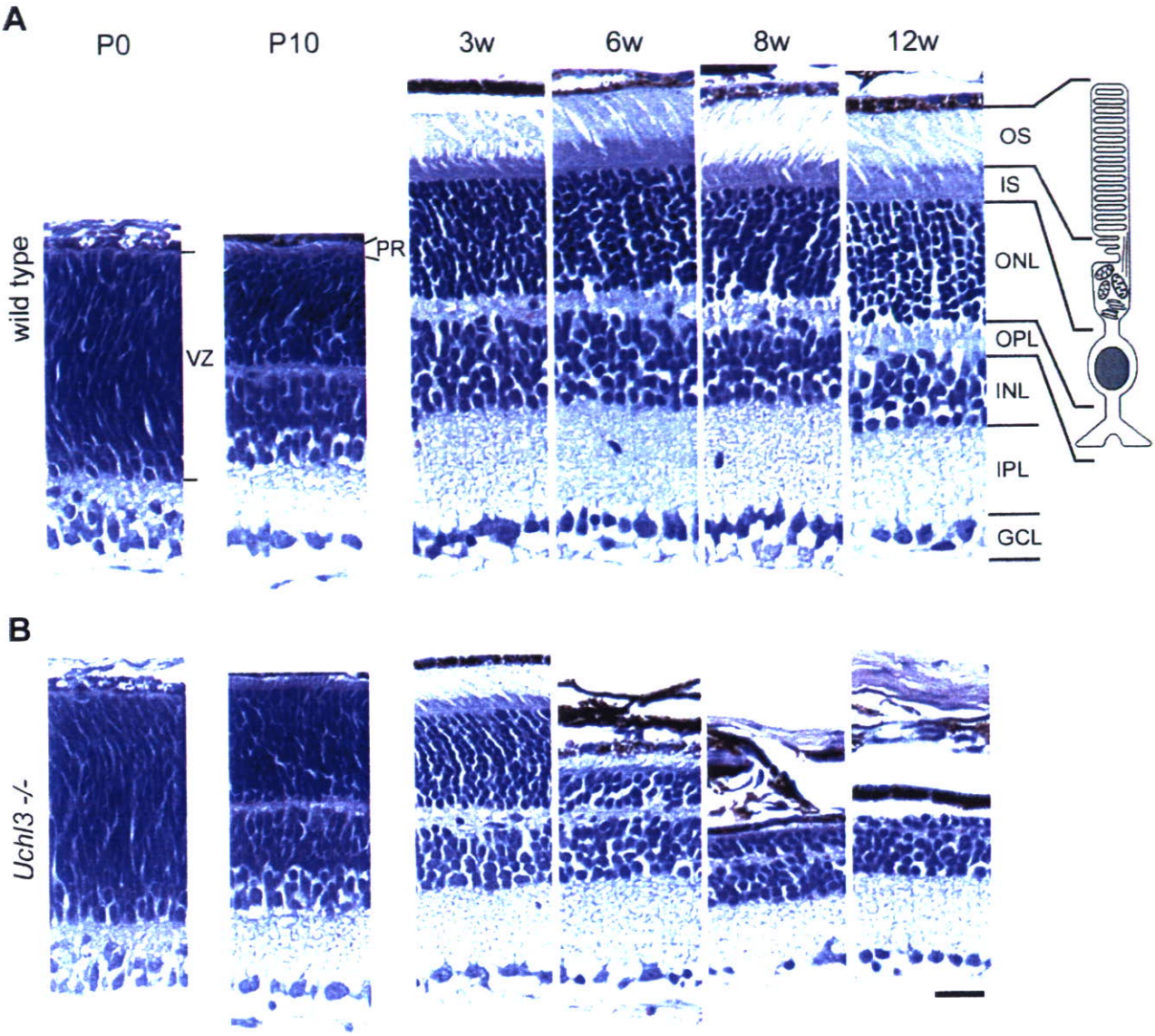

Figure 2. Histopathological changes of postnatal development in wild-type (**A**) and retinal degeneration of *Uchl3*-deficient mice (**B**) at P0, P10, 3w, 6w, 8w, and 12w. There is no morphological difference between both genotypes at P0 and P10, whereas outer and inner segments, outer nuclear layers, and outer plexiform layers are progressively degenerated after 3w of age. The illustration indicates a rod photoreceptor cell. VZ, ventricular zone; PR, photoreceptor; OS, outer segment; IS, inner segment; ONL, outer nuclear layer; OPL, outer plexiform layer; INL, inner nuclear layer; IPL, inner plexiform layer; GCL, ganglion cell layer. H&E staining. Scale bar = 20 μm (**A** and **B**).

6w, 8w, and 12w; for a total of 42 mice). The percentage of cristae area to whole mitochondrion in ultramicrophotographs was measured in 50 mitochondria of each genotype from three wild-type mice and four *Uchl3*-deficient mice, and the data were subjected to statistical analysis. All statistical analyses were carried out by Student's *t*-test using Microsoft Excel.

Results

Expression of UCH-L3 in the Murine Retina

Western blotting detected UCH-L3 (~30 kd) in extracts of eyes from wild-type mice at P10, 3w, and 6w, but the band was undetectable in *Uchl3*-deficient mice (Figure 1A). The expression level of UCH-L1 was similar in both genotypes. There was a tendency that the level of UCH-L3 decreased with age while the level of UCH-L1 increased with age in wild-type mice of all samples examined (five blots per antibody). Immunohistochemically, the cellular distribution of UCH-L3 differed from that of UCH-L1. UCH-L3 was enriched in the photoreceptor inner segment in wild-type mice at 3w of age (Figure 1B), whereas UCH-L1 was expressed in both genotypes in the inner retina, which consists of the inner nuclear layer, inner plexiform layer, and ganglion cell layer (Figure 1C). Localization of UCH-L3 in the wild-type retina was altered with age (Figure 1D). Immunoreactivity for UCH-L3 was not found at P0. UCH-L3 was faintly expressed in the outer plexiform layer at P10. Thereafter, it was localized to

inner segment at 3w. The inner segment was less immunoreactive for UCH-L3 at 6w, 8w, and 12w, compared with 3w.

Histopathological Changes of Retinal Degeneration in the Uchl3-Deficient Mice

Microscopic examination of retinal cross-sections revealed no obvious histopathological changes during early postnatal development at P0 and P10 in the retina of *Uchl3*-deficient mice (Figure 2). At 3w of age, the mutant retina began to degenerate in the inner segment and ultimately disappeared at 12w (Figures 2B and 3D). Thickness of the outer segment, outer nuclear layer, and outer plexiform layer was also significantly decreased in the mutant mice at 6w of age (Figure 3, C, E, and F). Despite the conspicuous change in the photoreceptor cells, the thickness of the mutant inner retina up to 12w of age was not altered compared with that of the wild-type (Figure 3, G–I).

Ultrastructurally, vacuolar changes were found in the inner segment of *Uchl3*-deficient mice at 3w of age (Figure 4). Mitochondria at the inner segment of mutant mice were slightly swollen. Groups of small round-to-oval structures were observed in the degenerated inner segment (Figure 4D), and these structures were considered to be the cross-sections of cell processes. Chromatin condensation in photoreceptor nuclei was sometimes seen in the outer nuclear layer at 3w (Figure 4F). Morphometric analysis showed that the percentage of cristae area to whole area of mitochondrion in the inner segment of *Uchl3*-deficient mice was significantly lower than that of wild-type mice (Figure 4, G and H).

Altered Expressions of Apoptosis-Related Proteins in the Degenerated Retina

Apoptotic cells in the retinal cross-sections were identified using the TUNEL staining. TUNEL-positive cells were identified in the ventricular zone at P0 and inner nuclear layer at P10 of both genotypes during the developmental period (Figure 5, A and C). The number of TUNEL-positive cells slightly increased in the inner nuclear layer at P10. After 3w of age, TUNEL-positive cells of mutant retina significantly increased at the outer nuclear layer of the mutant retina at 3w, 6w, and 8w (Figure 5, A and D).

To determine which apoptotic pathway was activated in *Uchl3*-deficient mice, we examined immunoreactivities of apoptosis-related proteins. Expression of cytochrome *c*, caspase-3, and cleaved caspase-3 and caspase-1, essential molecules for the caspase-dependent pathway, were unchanged in both genotypes (Figure 6A), whereas oxidative stress markers, COX and Mn-SOD as well as AIF and Endo G, indicators of the caspase-independent pathway, were altered in the mutant retina (Figure 6B). Chronological changes in expression of markers for oxidative stress and caspase-independent apoptosis at P0, P10, 3w, 6w, 8w, and 12w are shown in Table 1. The immunoreactivity of COX was increased in the inner segment at 3w and 6w. Mn-SOD was mildly increased in the inner segment at 3w, 6w, and 8w. Although AIF was enriched in the inner segment of *Uchl3*-deficient mice at 3w and 6w, nuclear labeling of AIF was not observed. On the other hand, Endo G was localized to the nuclei of the outer nuclear layer of the mutant retina at 3w and 6w. Expression of Endo G was slightly increased in the outer plexiform layer, inner nuclear layer, and inner plexiform layer of *Uchl3*-deficient mice after 3w of age (Table 1). Thus, degeneration of photoreceptor cells in *Uchl3*-defi-

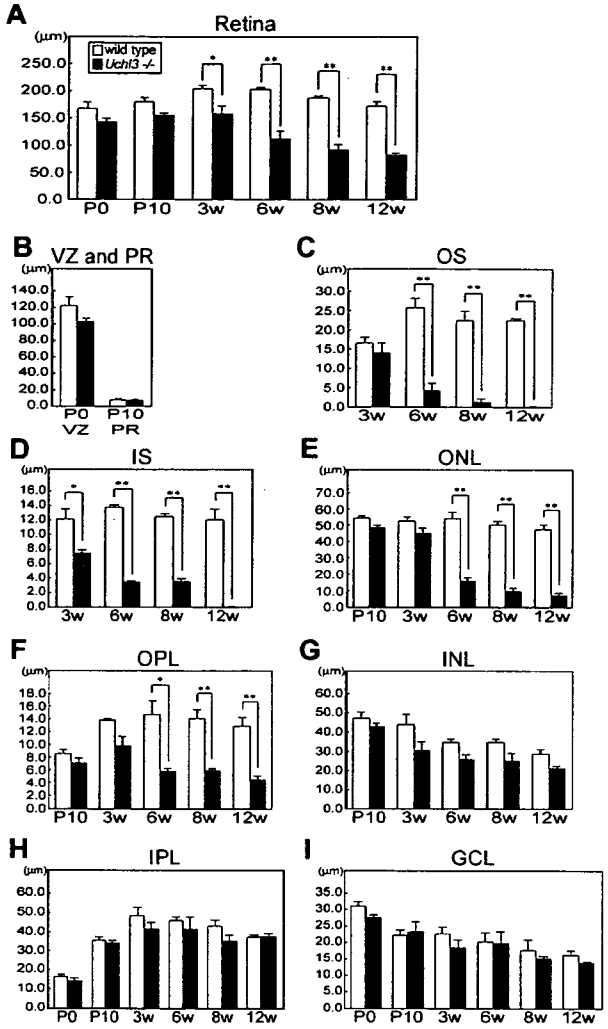

Figure 3. Chronological changes of retinal degeneration as assessed by thickness of each layer at different ages in wild-type and *Ucbl3*-deficient mice. **A:** Total retinal thickness is progressively decreased after 3w of age. **B:** Thickness of ventricular zone at P0 and photoreceptor layer at P10 shows no significant changes between both genotypes. **C–F:** Thickness of outer retinal layers in wild-type and *Ucbl3*-deficient mice at different ages. The earliest change is revealed at 3w of age in inner segment of mutant retina (**D**). Thickness of outer segment (**C**), outer nuclear layer (**E**), and outer plexiform layer (**F**) in *Uchl3*-deficient mice is significantly decreased with age compared with that in the wild-type. **G–I:** Thickness of inner retinal layers in wild-type and *Ucbl3*-deficient mice at different ages. Thickness of inner nuclear layer (**G**), inner plexiform layer (**H**), and ganglion cell layer (**I**) are unchanged between both genotypes. Each value represents the mean ± SE ($^{*}P < 0.05$; $^{**}P < 0.01$). In all panels, the white bars represent the thickness in wild-type mice and the black bars represent the thickness in *Uchl3*-deficient mice. VZ, ventricular zone; PR, photoreceptor; OS, outer segment; IS, inner segment; ONL, outer nuclear layer; OPL, outer plexiform layer; INL, inner nuclear layer; IPL, inner plexiform layer; GCL, ganglion cell layer.